nagra
National Cooperative for
the Disposal of Radioactive Waste

TECHNICAL REPORT 91-27

INTRAVAL TEST CASE 1B MODELLING RESULTS

A. JAKOB
J. HADERMANN

JULY 1991

PSI, Würenlingen and Villigen

Hardstrasse 73, CH-5430 Wettingen/Switzerland, Telephone + 42-56-37 11 11

nagra
National Cooperative for
the Disposal of Radioactive Waste

TECHNICAL REPORT 91-27

INTRAVAL TEST CASE 1B MODELLING RESULTS

A. JAKOB
J. HADERMANN

JULY 1991

PSI, Würenlingen and Villigen

Hardstrasse 73, CH-5430 Wettingen/Switzerland, Telephone + 42-56-37 11 11

This report was prepared as an account of work sponsored by Nagra. The viewpoints presented and conclusions reached are those of the author(s) and do not necessarily represent those of Nagra.

"Copyright (c) 1991 by Nagra, Wettingen (Switzerland). / All rights reserved.
All parts of this work are protected by copyright. Any utilisation outwith the remit of the copyright law is unlawful and liable to prosecution. This applies in particular to translations, storage and processing in electronic systems and programs, microfilms, reproductions, etc."

Table of Contents

Vorwort

Im Rahmen des Programmes Entsorgung werden im PSI Arbeiten zur Analyse der Ausbreitung radioaktiver Elemente in geologischen Medien durchgeführt. Diese Untersuchungen werden in Zusammenarbeit und mit teilweiser finanzieller Unterstützung der Nationalen Genossenschaft für die Endlagerung radioaktiver Abfälle (NAGRA) vorgenommen. Die vorliegende Arbeit erscheint gleichzeitig als PSI–Bericht und als NAGRA Technischer Bericht.

Abstract

This report presents results obtained within Phase I of the INTRAVAL study.
Six different models are fitted to the results of four infiltration experiments with ^{233}U tracer on small samples of crystalline bore cores originating from deep drillings in Northern Switzerland.
Four of these are dual porosity media models taking into account advection and dispersion in water conducting zones (either tubelike veins or planar fractures), matrix diffusion out of these into pores of the solid phase, and either non–linear or linear sorption of the tracer onto inner surfaces. The remaining two are equivalent porous media models (excluding matrix diffusion) including either non–linear sorption onto surfaces of a single fissure family or linear sorption onto surfaces of several different fissure families.
The fits to the experimental data have been carried out by a Marquardt–Levenberg procedure yielding error estimates of the parameters, correlation coefficients and also, as a measure for the goodness of the fits, the minimum values of the χ^2 merit function. The effects of different upstream boundary conditions are demonstrated and the penetration depth for matrix diffusion is discussed briefly for both alternative flow path scenarios.
The calculations show that the dual porosity media models are significantly more appropriate to the experimental data than the single porosity media concepts. Moreover, it is matrix diffusion rather than the non–linearity of the sorption isotherm which is responsible for the tailing part of the break–through curves. The extracted parameter values for some models for both the linear and non–linear (Freundlich) sorption isotherms are consistent with the results of independent static batch sorption experiments. From the fits, it is generally not possible to discriminate between the two alternative flow path geometries.
On the basis of the modelling results, some proposals for further experiments are presented.

Zusammenfassung

Dieser Bericht präsentiert die Resultate, die für INTRAVAL Phase I erarbeitet wurden.
Sechs verschiedene Modelle werden an den Resultaten von vier Infiltrationsexperimenten gefittet. Diese wurden, mit ^{233}U als Tracer, durchgeführt an Ausschnitten von Bohrkernen aus kristallinem Gestein, die von Tiefbohrungen in der Nord–Schweiz stammen.
Vier der theoretischen Ansätze sind Modelle für das "doppelt poröse Medium" unter Berücksichtigung von Advektion und Dispersion in den wasserführenden Zonen (entweder röhrenförmige Adern oder planare Spalten); Matrixdiffusion aus diesen Zonen heraus in Porenräume der Festphase und entweder nicht–lineare oder lineare Sorption an inneren Oberflächen. Die anderen zwei Konzepte sind Modelle für das "äquivalent poröse Medium" (also unter Ausschluss von Matrixdiffusion) mit Berücksichtigung entweder nicht–linearer Sorption an Oberflächen eines einzelnen Spalttypus oder lineare Sorption an Oberflächen mehrerer verschiedener Spaltfamilien.
Die Anpassung an die experimentellen Werte werden mit Hilfe eines Marquardt–Levenberg Verfahrens vorgenommen; dabei erhält man Fehlerabschätzungen für die Fit–Parameterwerte, Korrelationskoeffizienten und – als ein Mass für die Güte der Fits – χ^2–Minimumswerte.
Für beide Fliessgeometrien wird der Einfluss verschiedener Randbedingungen am Eingang aufgezeigt, und es wird auch auf die Eindringtiefe für die Matrixdiffusion kurz eingegangen.
Die Rechnungen zeigen, dass die Modelle für das "doppelt poröse Medium" die experimentellen Daten deutlich besser reproduzieren als die Konzepte für das "äquivalent poröse Medium". Überdies lassen die Rechnungen erkennen, dass eher die Matrixdiffusion als die Nicht–Linearität der Sorptionsisotherme verantwortlich ist für das Langzeitverhalten der Durchbruchskurven. Die extrahierten Parameterwerte für beide, die lineare wie auch die nicht–lineare (Freundlich) Sorptionsisotherme sind verträglich mit Werten aus unabhängigen, statischen Sorptionsexperimenten. Hingegen ist es im allgemeinen nicht möglich, aufgrund der Best–Fits, zwischen den beiden alternativen Fliessweg–Geometrien zu unterscheiden.
Ausgehend von den Resultaten werden Vorschläge für zukünftige Experimente gemacht.

Riassunto

Questo referto presenta risultati ottenuti nell'ambito dello studio INTRAVAL, fase I. Sei modelli distinti vengono adattati ai risultati di quattro esperimenti di infiltrazione col tracciante ^{233}U. Gli esperimenti sono stati condotti su piccoli campioni di roccia cristallina provenienti da perforazioni a grande profondità eseguite nella Svizzera settentrionale.
I primi quattro modelli postulano, per un mezzo a doppia porosità, i seguenti processi: trasporto avvettivo e dispersione nelle zone acquifere (condotti tubulari o fratture planari), diffusione dalle zone suddette nello spazio poroso della matrice solida incassante ed assorbimento lineare o non lineare sulle superfici interne della matrice. I rimanenti due modelli postulano un unico mezzo a porosità equivalente, escludono la diffusione nella matrice, e richiedono assorbimento non lineare su superfici di un' unica famiglia di fessura, oppure assorbimento lineare su superfici di diverse famiglie di fessure.
Gli adattamenti ai dati sperimentali sono stati ottenuti attraverso il procedimento di Marquardt–Levenberg, che fornisce stime sugli errori dei parametri, coefficienti di correlazione e, quale misura della qualità degli adattamenti, il valore minimo della funzione χ^2. Si dimostrano le conseguenze della scelta di diverse condizioni limite all' entrata del condotto. Si discutono brevemente i valori della profondità di penetrazione per diffusione nella matrice ottenuti con due vie di deflusso alternative.
I risultati indicano che i modelli a doppia porosità sono più appropriati dei modelli a porosità singola nel riprodurre i dati sperimentali.
Inoltre, la posizione dei dati sperimentali nella coda della curva di rottura può essere spiegata ipotizzando diffusione nella matrice, ma non assumendo un' isoterma di assorbimento non lineare. I valori dei parametri ottenuti per entrambe le isoterme di assorbimento (lineare e non lineare (Freundlich)) sono compatibili coi risultati di esperimenti indipendenti. Tuttavia, non é possibile distinguere, in base ai valori calcolati, tra le due geometrie di deflusso. A partire dai risultati ottenuti, vengono avanzate proposte per esperimenti futuri.

Resumé

Le rapport présente des résultats obtenus dans le cadre de l'étude INTRAVAL, phase I.
Six modèles différents ont été adaptés aux résultats de quatre essais d'infiltration au traceur ^{233}U. Les essais ont été conduits sur des petits échantillons de roche crystalline provenants de perforations profondes effectuées dans le nord de la Suisse.
Les premiers quatre modèles hypotisent, pour un milieu à double porosité les procès suivants: transport par advection et dispérsion dans les zones aquifères (conduits tubulaires ou fractures plaines), diffusion de dites zones dans les pores de la roche adjointe et adsorption linéaire ou non linéaire sur les surfaces internes de la matrice. Les autres deux modèles hypothisent un seul milieu à porosité équivalente et excluent la diffusion dans la matrice. Ils demandent l'adsorption non linéaire sur les surfaces d'une seule famille de fissures, ou bien l'adsorption linéaire sur surfaces de différentes famillies de fissure.
L'adaption à les données expérimentales à été obtenue grâce à la méthode de Marquardt–Levenberg, qui fournit des estimations sur les erreurs des paramètres des coefficients de corrélation et, pour la mesure de la qualité des adaptations, la valeur minimale de la fonction χ^2. On montre les conséquences du choix de différentes conditions limite à l'entrée du conduit. On discute les valeurs de la profondité de pénetration par diffusion dans la matrice obtenues avec deux voies d'écoulement altérnatives.
Les résultats montrent que les modèles à double porosité réproduisent les données expérimentales mieux que ceux à porosité unique.
En outre, la position des données expérimentales dans la queue des courbes d'écoulement peut être éxpliquée en hypothisant diffusion dans la matrice, mais non par une isothèrme d'adsorption non linéaire. Les valeurs des paramètres obtenus pour les deux isothèrmes (linéaire et non linéaire (Freundlich)) sont en accord avec les resultats d'essais indépentants. Cependant, il n'est pas possible, sur la base des valeurs calculées, de distinguer entre les deux géometries d'écoulement. Sur la base des résultats obtenus, ont fait des propositions pour les essais futurs.

1 Introduction

Nuclear power stations, industry, research centres and hospitals produce radioactive waste which must be disposed of in a safe way. Parts of the waste contain nuclides with very long (compared to human life time) half–lives and have therefore to be isolated from man and his environment for a very long period. In Switzerland, one possibility is to deposit this waste in deep lying stable underground formations of crystalline rock such as granite or gneiss. Crystalline formations are an attractive option for disposal over very long time periods due to their stability, relatively simply geochemistry and their lack of valuable minerals, making human intrusion in the future unlikely, and due to the multitude of investigations performed worldwide in the last decade. A further advantage is the capacity of crystalline rock to retard the transport of released radionuclides in the groundwater by a variety of mechanisms.
The most likely mechanisms to return radionuclides to the biosphere from a repository is dissolution and transport in flowing groundwater. Extensive studies in many countries have therefore been undertaken to determine and to describe the important mechanisms which govern solute transport.
In order to apply various models and fix the most sensitive parameters, suitable experiments on a variety of distance and time scales, such as small–scale laboratory experiments, large–scale field experiments or studies on natural analogues, have to be performed. For theorists, the analysis and interpretation of data from laboratory/field experiments constitutes an important part of their work.
This report describes the modelling work done at PSI in connection with test case 1b of INTRAVAL[†]: uranium infiltration through bore cores from deep crystalline rock in Northern Switzerland. A first interpretation considering two models, only, has been presented (outside the INTRAVAL study) previously [2].
The advantage of laboratory experiments is the possibility of achieving well–defined initial and boundary conditions. Individual processes can often be more easily identified and the experimental set–up can be designed to allow parameter variations. Relatively economical laboratory experiments provide data for the interpretation of larger (and more expensive) field experiments. On the other hand there are also disadvantages worth mentioning: the temporal and spatial scales are many orders of magnitude smaller than those required in, for example, a safety assessment study. Moreover, difficulties in the experimental techniques and sample preparation often yield incomplete or inadequate data for the analysis by a modeller. Nevertheless, experiments like test case 1b and the subsequent theoretical analysis are important and inseparable from the study of phenomena like dispersion, channelling, matrix diffusion, sorption, geometries of flow paths, effects of stress changes and so on.

The main questions for the present modelling work were:

- What are the dominant mechanisms required to describe the experiments?
- Which are the geometrical factors affecting nuclide transport?
- Can we discriminate between differing assumptions concerning processes and geometries?
- What further experiments should be performed to resolve open questions?

We have applied six different transport models to all four infiltration experiments making up test case 1b. The fit to the experimental breakthrough curves has been carried out using a Marquardt–Levenberg procedure.

The paper is organised as follows: In the next section we present briefly (and for completeness) the salient features of the experiment. The models are described in section 3, results and discussions follow in section 4 and conclusions and proposals for further experimentation are given in section 5.

[†]The international INTRAVAL project [1] started in October 1987 in Stockholm as an international effort towards "validation" of geosphere models for transport of radionuclides.

2 Experiments

For completeness we present in this section a short description of the ^{233}U infiltration experiments. These work has been performed at PSI and is reported in detail in [3].
Several cylindrical rock samples have been cut out from deep drilling bore cores from crystalline in Northern Switzerland. In Table 1 a short characterisation, compiled from [3], of each of the samples and their geometrical dimensions is listed.

Signature of the sample	Location and depth [m] below the surface	Lithology (rock type)	Core diameter $\Phi \cdot 10^2$ [m]	Core length $L \cdot 10^2$ [m]
KAI817	Kaisten, 817.56	fresh sillimanite – cordierite – biotite gneiss with visible axial microfissure	4.60	1.16
BOE856R	Böttstein, 856.56	sericitised – albitised granite with microfractures cemented by clay and calcite	4.60	1.45
BOE856R2	Böttstein, 856.68		4.60	1.52
BOE1093	Böttstein, 1093.81	fresh granite	4.60	2.07

Table 1: Location, depth, characterisation of the rock type, core diameter and length for all four samples.

For the infiltration experiment, the sample was placed in a pressurised rig schematically described in Figure 1, taken from ref. [3].
The sample was mounted between two end–pieces and held in position with a flexible rubber sleeve. Each cylindrical end–piece is made out of stainless steel, with a central bore ending in a spiral groove in the face in contact with the rock sample. The end–pieces and the grooves distribute both axial stress and the infiltration liquid over the upstream face of the sample and collect the outflowing solution at the downstream face.
The core assembly was placed in the pressure vessel. A confining pressure (simulating a lithostatic pressure) and an infiltration pressure were maintained by external pumps. The infiltration fluid was natural granitic groundwater from Bad Säckingen, Germany. After conditioning the sample (i.e. when a steady flow rate of infiltration fluid had been reached), the valve was opened for a short time (with respect to transport times) in order to inject a measured rectangular input pulse of ^{233}U dissolved in distilled water[†]. At the downstream side, the eluting solution was sampled in fractions (a given number of drops) continuously monitoring the electrical conductivity and pressures. Drop and fraction events were recorded, the uranium concentration (radioactivity) has been measured batch–wise. After terminating the infiltration experiment, the aparatus was dismantled and the sample cut transversely or longitudinally into slices of about 1 mm thickness. Both surfaces of each slice were alpha–autoradiographed in order to obtain information on the spatial distribution of flow paths and sorption sites.

[†]The pH of the solution, adjusted with NaOH, was 7.9 – 8.1.

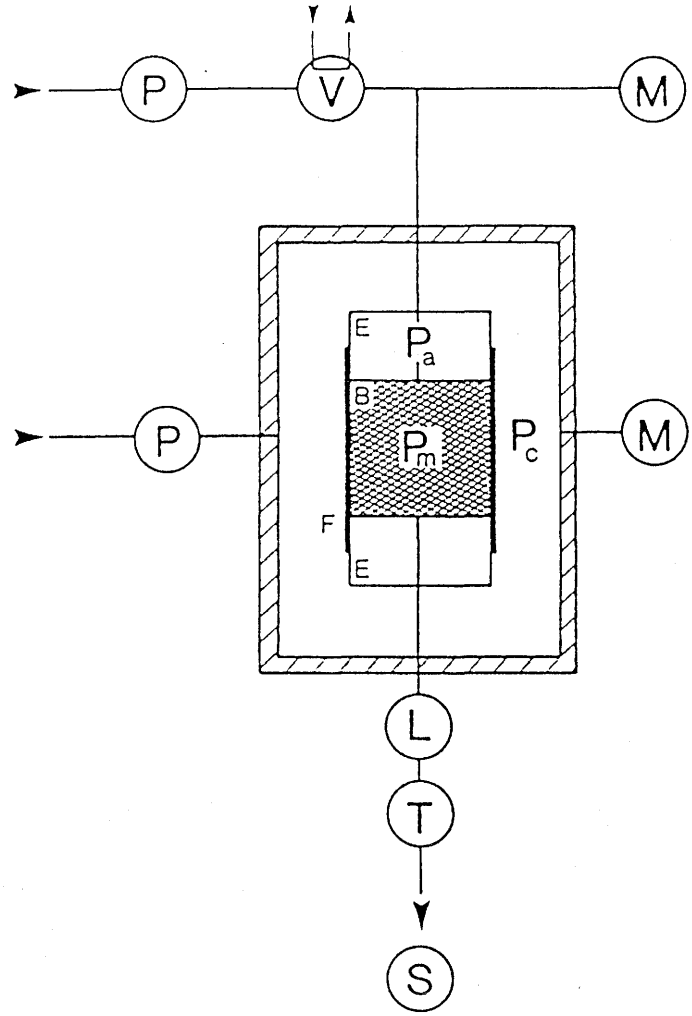

FIGURE 1. Schematic diagram of pressure infiltration apparatus with the following components: Core assembly with (B) core sample, (E) end pieces, (F) flexible sleeve, (P) hydraulic pumps, (M) manometers, (V) injection valve, (L) electrical conductivity monitor, (T) droplet counter, (S) fraction/droplet sampler, (Pc) confining pressure (0–600 bar), (Pa) infiltration pressure (0–230 bar), (Pm) pore pressure.

Data given to projects teams were:

- diameter and length of the cylindrical samples
- weight of water–saturated sample
- weight of dry sample
- specific weight of the sample
- effective porosity of the sample
- mineral composition of the rock cores
- confining pressure
- infiltration pressure
- dead volume of flow system
- hydraulic conductivity as a function of the confining pressure
- dynamic porosity as a function of the confining pressure
- total number of fractions collected
- number of drops per fraction
- drop frequency
- mean drop volume (or mean weight of drop)
- mean flow rate
- mass of tracer spike
- volume of tracer spike
- input concentration of ^{233}U
- electrical conductivity as a function of time
- concentration of ^{233}U in each fraction
- activity of each fraction as a function of time, normalised to the input concentration
- results from alpha–autoradiography of the surfaces of the slices
- from independent experiments: uranium(VI)–sorption data on crushed material from the Grimsel Test Site

We also mention some essential difficulties with respect to an interpretation of the experiments:

- During the experiment a confining pressure corresponding to the original lithostatic pressure is applied to the sample. Experiments varying the pressures show that this has little effect on the porosity but causes changes in the hydraulic conductivity [3]. These changes are irreversible and the sample may not be in equilibrium during infiltration.
- The chemistry of the porewater of all the samples is not known. For the experiment, an alternative granitic groundwater was used. This reference water is highly mineralised and consists of both granitic deep water and groundwater from close to the surface [4]. The change in chemistry may give rise to geochemical reactions within the rock sample, producing time–dependent transport parameters. A hint of the presence of such effects is the decreased permeability during the experiments (another explanation could be precipitation of the tracer). In some experiments the infiltration pressure was increased, increasing the water flow rate, to counteract the decreased permeability and to limit the duration of the experiment.
- At the upstream end–piece near the bore, the tracer starts migrating into the rock before it reaches the outer part of the spiral. This effect gives rise to a curved tracer front in the sample[†]. In other words, the time dependence of the ^{233}U input function is not well known (see also sub–chapter 4.3). Nevertheless, for the modelling work we assume a step (constant) input over a certain time period. This seems justified if transport times are large with respect to tracer input times and the dispersivity is sufficiently small.

[†]A similar process reinforces the effect at the outlet end–piece. The spiral grooves of both end–pieces retard the tracer pulse. The greater the distance from the bore the greater the retardation.

3 Model equations

Based on the mass balance for a REV [5], one can formulate a system of coupled non–linear partial differential equations for nuclide transport in a dual porosity medium in which we differentiate between a fracture and a vein geometry for the water conducting zones:

$$\frac{\partial C_f}{\partial t} = \sum_{j=1}^{M} \alpha^{(j)} \frac{\partial C_f^{(j)}}{\partial t}$$

$$= \sum_{j=1}^{M} \frac{\alpha^{(j)}}{R_f^{(j)}(C_{f,tot}^{(j)})} \left[a_L^{(j)} v_f^{(j)} \frac{\partial^2 C_f^{(j)}}{\partial z^2} - v_f^{(j)} \frac{\partial C_f^{(j)}}{\partial z} + \left\{ \begin{array}{l} \frac{1}{b^{(j)}} \epsilon_p^{(j)} D_p^{(j)} \frac{\partial C_p^{(j)}}{\partial x} \Big/_{|x| = b^{(j)}} \\ \frac{2}{R^{(j)}} \epsilon_p^{(j)} D_p^{(j)} \frac{\partial C_p^{(j)}}{\partial r} \Big/_{r = R^{(j)}} \end{array} \right. \right. \begin{array}{l} \text{(for fract} \\ \text{(for veins} \end{array} \tag{3.1}$$

$$\frac{\partial C_p^{(j)}}{\partial t} = \frac{D_p^{(j)}}{R_p^{(j)}(C_{p,tot}^{(j)})} \left\{ \begin{array}{ll} \frac{\partial^2 C_p^{(j)}}{\partial x^2} & \text{(for fractures)} \\ \left(\frac{\partial^2 C_p^{(j)}}{\partial r^2} + \frac{1}{r} \frac{\partial C_p^{(j)}}{\partial r} \right) & \text{(for veins)} \end{array} \right. \tag{3.2}$$

We use the following notation:

C_f	...	concentration of the nuclide in the flowing water [mol · m^{-3}]
$C_{f,tot}^{(j)}$	...	cumulative nuclide concentration of $C_f^{(j)}$ and C_{min} in the flowing water of the j-th fracture/vein family [mol · m^{-3}]
$C_{p,tot}^{(j)}$	...	cumulative nuclide concentration of $C_p^{(j)}$ and C_{min} in the pore water of the matrix for the j-th fracture/vein family [mol · m^{-3}]
$C_f^{(j)}$	...	concentration of the nuclide in the flowing water of the j-th fracture/vein family [mol · m^{-3}]
$C_p^{(j)}$	...	concentration of the nuclide in the pore water of the matrix for the j-th fracture/vein family [mol · m^{-3}]
C_{min}	...	natural nuclide concentration [mol · m^{-3}]
$R_f^{(j)}(C_{f,tot}^{(j)})$	...	retention function in the j-th fracture/vein family
$R_p^{(j)}(C_{p,tot}^{(j)})$	...	retention function in the matrix for the j-th fracture/vein family
$\alpha^{(j)}$	...	weighing factor for the j-th fracture/vein family
$a_L^{(j)}$	...	longitudinal dispersion length for the j-th fracture/vein family [m]
$v_f^{(j)}$	...	water velocity in the j-th fracture/vein family [m·s^{-1}]
$b^{(j)}$	...	j-th fracture half–width [m]
$R^{(j)}$	...	j-th vein radius [m]
$\epsilon_p^{(j)}$	...	effective porosity of the rock matrix for the j-th fracture/vein family [–]
$D_p^{(j)}$	...	diffusion constant in the rock matrix for the j-th fracture/vein family [m^{2}s^{-1}]

The first equation (3.1) describes the transport of the nuclide as linear superposition of transport within M independent water carrying zones with weighing factors $\alpha^{(j)}$. We consider two alternative scenarios: either (x,z)–Cartesian geometry for transport in fractures or (r,z)–cylindrical geometry for transport in veins.
The second equation (3.2) represents the molecular diffusion of the tracer into stagnant water of the adjacent rock matrix, whereby lateral diffusion is always neglected.
Both equations are coupled by the third term on the right hand side of eq. (3.1) – the diffusive term describing diffusion across the boundary. In modelling the present experiments, radioactive decay of the tracer can be neglected.

For the weights in eq. (3.1), the following relation holds:

$$\sum_{j=1}^{M} \alpha^{(j)} = 1 \quad . \tag{3.3}$$

and for the specific discharge q [m/s]:

$$q = \sum_{j=1}^{M} \alpha^{(j)} \epsilon_f^{(j)} v_f^{(j)}$$

where $\epsilon_f^{(j)}$ [–] is the flow porosity for the j-th fracture/vein family†. Matrix porosities $\epsilon_p^{(j)}$ add up to the total matrix porosity. The relationship is dependent on the geometrical structure and the maximum possible penetration depths for matrix diffusion.

Sorption of the tracer on the fracture (vein) surfaces, and also on inner surfaces of the rock matrix may be concentration dependent. We use the well–known phenomenological relationship by Freundlich:

$$S_{f,p}^{(j)} = K_{f,p}^{(j)} \cdot C_{f,p}^{(j)\,N_{f,p}^{(j)}} . \tag{3.4}$$

S describes the nuclide concentration either on the fracture (vein) surfaces [mol/m^2] (index f), or, with index p, the concentration [mol/kg] on the pore surfaces of the rock matrix. K is the Freundlich coefficient and has the unit [mol$^{1-N_f}$m$^{3N_f-2}$] in the fracture (vein), and [mol$^{1-N_p}$m^{3N_p}kg^{-1}] in the matrix, N being the Freundlich exponent. The retention function in a fracture or vein is given by:

$$R_f^{(j)}(C_{f,tot}^{(j)}) := \begin{cases} 1 + \dfrac{1}{b^{(j)}} K_f^{(j)} N_f^{(j)} C_{f,tot}^{(j)\,N_f^{(j)}-1} & \text{(for fractures)} \\ 1 + \dfrac{2}{R^{(j)}} K_f^{(j)} N_f^{(j)} C_{f,tot}^{(j)\,N_f^{(j)}-1} & \text{(for veins)} \end{cases} \tag{3.5}$$

and by:

$$R_p^{(j)}(C_{p,tot}^{(j)}) := 1 + \frac{1-\epsilon_p^{(j)}}{\epsilon_p^{(j)}} \rho K_p^{(j)} N_p^{(j)} C_{p,tot}^{(j)\,N_p^{(j)}-1} \tag{3.6}$$

in the matrix where the index tot indicates total†† elemental concentration and ρ [kg/m^3] is the solid phase density.

---

†For the model with $M > 1$ (model 4, see also page 13) we shall implicitely assume that all water–velocities $v_f^{(j)}$ are equal and shall vary only the retardation factors $R_f^{(j)}$. This seems reasonable since only the ratio $v_f^{(j)}/R_f^{(j)}$ enters the equations.

††The infiltration water has a natural uranium concentration C_{min} of $1.1 \cdot 10^{-2}$ mg/l [6]. If the ^{233}U concentration is below C_{min}, the sorption processes are dominated by isotopic exchange, which are described by a linear sorption isotherm resulting in constant retention factors. Therefore, the cumulative concentration $C_{f,p;tot}^{(j)} = C_{f,p}^{(j)} + C_{min}$ enters eqs. (3.5) and (3.6).

For $N_{f,p}^{(j)} \equiv 1$ one gets the linear isotherms with:

$$\begin{aligned} K_f^{(j)} &\equiv K_a^{(j)} \quad [\mathrm{m}] \\ K_p^{(j)} &\equiv K_d^{(j)} \quad [\mathrm{m^3/kg}]. \end{aligned}$$

To solve the system of differential equations, eqs. (3.1) and (3.2), suitable initial and boundary conditions have to be specified.

Initial conditions:

$$C_f^{(j)}(z,t) = \begin{cases} C_p^{(j)}(x,t) = 0 & |\, x \,| \geq b^{(j)} \\ C_p^{(j)}(r,t) & r \geq R^{(j)} \end{cases} \quad ;t \leq 0 \;\; ;\forall j \qquad \begin{matrix} \text{(for fractures)} \\ \text{(for veins)} \end{matrix} \tag{3.7}$$

Boundary conditions:

Due to the special physical problem the (general) mixed von–Neumann/Dirichlet boundary conditions are reduced to the following expressions:

a) Inlet (Upstream)

$$C_f^{(j)}(z = 0, t > 0) = C_\circ \cdot \Theta(T_L - t) \tag{3.8}$$

where:
$$\Theta(t') = \begin{cases} 0 \;\; ; \;\; t' < 0 \\ 1 \;\; ; \;\; t' \geq 0 \end{cases}$$

$C_\circ$ is the (constant) tracer input concentration [mol/m^3] maintained for the infiltration duration T_L [s]†.

b) Outlet (Downstream)

$$\frac{\partial C_f^{(j)}(z = L, t > 0)}{\partial z} = 0 \tag{3.9}$$

This corresponds to free outflow at the outlet.

†This upstream boundary conditions does not preserve mass conservation, but may be a good approximation. See also section 4.3 (page 31)

c) Matrix

In the surrounding rock matrix we choose as boundary condition at a certain distance $D^{(j)}$ [m] the maximum possible penetration depth for matrix diffusion‡:

$$\left.\begin{array}{l} D_p^{(j)} \dfrac{\partial C_p^{(j)}}{\partial x} \Big/_{|x|=D^{(j)}} \\ D_p^{(j)} \dfrac{\partial C_p^{(j)}}{\partial r} \Big/_{r=D^{(j)}} \end{array}\right\} = 0 \qquad \begin{array}{l} \text{(for fractures)} \\ \text{(for veins)} \end{array} \tag{3.10}$$

The concentration is continuous across the interface of the water–conducting zone and the rock matrix:

$$\left.\begin{array}{l} C_p^{(j)}(b^{(j)},t) \\ C_p^{(j)}(R^{(j)},t) \end{array}\right\} = C_f^{(j)}(z,t) \qquad \forall z,t>0 \qquad \begin{array}{l} \text{(for fractures)} \\ \text{(for veins)} \end{array} \tag{3.11}$$

Eqs. (3.1) and (3.2) are solved numerically with the code RANCHMDNL, which is described in detail in [7].

From the basic equations (3.1) and (3.2), one can easily develop four different models for tracer transport:

Model 1: dual porosity medium† (including matrix diffusion) with non–linear sorption. Advective transport may occur either in fractures or veins.

Model 2: dual porosity medium† (including matrix diffusion) with linear sorption. Again the two flow–path geometries are distinguished.

Model 3: equivalent porous medium†† (excluding matrix diffusion) with non–linear sorption onto fissure or vein surfaces§.

Model 4: superposition of several equivalent porous media†† (excluding matrix diffusion) with linear sorption onto fissure or vein surfaces§.

---

‡For more details for the definition of $D^{(j)}$ we refer to the discussion below (see also page 15 and to sub–chapter 4.4 page 33)

†In a **dual porosity medium** we consider three regions within the rock:

- a fluid–conducting zone with aperture (fracture width) $2b$ in which transport occurs through advection and dispersion. The radionuclides are retarded by sorption processes on fissure surfaces.
- a zone with thickness D of rock with connected pore spaces. In this volume, advection and dispersion are neglected and transport is only due to molecular diffusion. Additionally, the nuclides may be retarded by sorption processes onto inner surfaces. If diffusion in the altered rock zones is sufficiently fast [8] such that $C_p^{(j)}(x,t) = C_f^{(j)}(z,t) \quad \forall x,z \le D; \quad \forall t$ the dual porosity medium degenerates to the equivalent porous medium approach (see also [8]).
- rock region with no connected porosity and hence where one can neglect tracer transport.

††In a **equivalent porous medium** we distinguish two regions within the rock:

- a fluid–conducting zone in which transport occurs through advection and dispersion. The radionuclides are retarded by sorption processes on fissure surfaces.
- rock region with no connected porosity and hence where one can neglect tracer transport.

§Note that the two geometries cannot be distinguished.

One obtains the transport equations for each model from eqs. (3.1) and (3.2), with the help of the table 2: (Note, for $M \equiv 1$ the summation index j is omitted.)

Model no.	M	$D_p^{(j)}$	$N_f^{(j)}$	$N_p^{(j)}$	Number of flow path geometries
1	1	> 0	$0 < N_f < 1$	$0 < N_p < 1$	2
2	1	> 0	1	1	2
3	1	0	$0 < N_f < 1$	–	1
4	> 1	0	1	–	1

Table 2: Values and ranges of some parameters of eqs. (3.1) and (3.2) for the four different models
(A bar indicates that for this model the parameter does not occur in the transport equations.)

The solutions to eqs. (3.1) and (3.2) have been fitted to the experimental time history of the concentrations of ^{233}U for all four bore–cores. For the fit procedure we used the Marquardt–Levenberg method [9] by minimisation of the χ^2 merit function, except in the case of model 4 calculations, where simple fits–by–eye were carried out. One can obtain regression parameters, their standard deviations and the corresponding correlation matrix.

Values for the experimental data are taken from [3] and listed below in Table 3:

Core sample	$v_f \cdot 10^6$ [m/s]	$\epsilon_p \cdot 10^3$ [–]	$\overline{\rho} = \rho(1-\epsilon_p)$ [kg/m^3]	$C_0 \cdot 10^3$ [mol/m^3]	T_L [s]
KAI817	8.81	37	2700	38.4	849
BOE856R	3.98	15	2550	38.4	963
BOE856R2	10.4	32	2520	38.4	829
BOE1093	9.63	7	2600	38.4	773

Table 3: Water–velocities, matrix porosities, bulk rock densities, input concentrations and tracer injection times for the four rock samples

There have been many laboratory experiments in which the effective diffusion constant has been determined in crystalline rocks (see also [10] and references therein). A reasonable range is:

$$10^{-14} \leq \epsilon_p D_p \leq 10^{-12} \quad [\mathrm{m}^2/\mathrm{s}]$$

We fix its value for the present work to: $\epsilon_p D_p = 10^{-13}$ [m^2/s].

Currently, we see no possibility of fixing the fracture apertures $b^{(j)}$ or the vein radii $R^{(j)}$ from independent (experimental) information. For the calculations, we have chosen the previously fitted values listed in Table 4, taken from [2]. It should be noted, however, that for a strongly sorbing nuclide such as uranium the results are virtually independent of the values of $b^{(j)}$ and $R^{(j)}$ and for a fixed specific discharge.

Core sample	$b^{(j)} \cdot 10^5$ [m]	$R^{(j)} \cdot 10^5$ [m]
KAI817	4.55	4.55
BOE856R	1.00	2.00
BOE856R2	0.50	1.00
BOE1093	0.40	0.80

Table 4: Fracture half–width and vein radius for all four bore cores

For the maximum penetration depth $D^{(j)}$ for matrix diffusion, we have chosen a value such that the no–flow boundary condition eq. (3.10) acts far in the matrix and the value of $D^{(j)}$ does not influence the results. One can show [11] that in this case – this means: for large $D^{(j)}$ – and for linear sorption isotherms (model 2) there are only three independent parameters†. In the following table, the free parameters are listed for every model.

Model	$\alpha^{(j)}$	$a_L^{(j)}$	$R_f^{(j)}$	$K_f^{(j)}$	$N_f^{(j)}$	$K_d^{(j)}$	$K_p^{(j)}$	$N_p^{(j)}$	Number of free parameters
1		x		x	(x)		x	(x)	5 (3)
2		x	x			x			3
3		x		x	x				3
4	x	x	x						3M-1

Table 5: Table of fit parameters. The brackets indicate that these parameters have been fixed for one set of calculations (model 1a).

†We would like to thank L. Moreno for pointing this out to us.

4 Results and Discussion

4.1 Results

In this section we present the comparison of theoretical results and experimental data. A somewhat more detailed discussion will follow in the subsequent subsections. Table 6 shows all the fitted parameters together with their standard deviations and the minimum values of the χ^2 merit functions for all the models, with the exception of model 4 where only fits–by–eye has been performed. The uncertainties in the values of the parameters are derived from the diagonal elements of the covariance matrix. Again, we omit, in the second column, the (upper) summation index j if $M \equiv 1$. This is the case for all except model 4.

Model	Parameter		KAI817		BOE856R		BOE856R2		BOE1093	
			fracture flow	vein flow	fracture flow	vein flow	fracture flow	vein flow	fracture flow	vein flow
Model 1 Dual porosity medium; non–linear sorption	$a_L \cdot 10^3$ $K_f \cdot 10^4$ N_f $K_p \cdot 10^3$ N_p $\chi^2_{min} \cdot 10^5$	[m] $[\mathrm{mol}^{1-N_f}\mathrm{m}^{3N_f-2}]$ [–] $[\mathrm{mol}^{1-N_p}\mathrm{m}^{3N_p}\mathrm{kg}^{-1}]$ [–] [–]	0.37 ± 0.09 0.43 ± 0.1 0.63 ± 0.03 7.9 ± 2.6 0.53 ± 0.05 0.13	0.95 ± 0.16 0.47 ± 0.06 0.70 ± 0.02 3.9 ± 1.3 0.64 ± 0.04 0.22	0.36 ± 0.24 0.36 ± 0.06 1.1 ± 0.1 0.079 ± 0.012 0.46 ± 0.03 0.091	4.3 ± 1.2 0.37 ± 0.04 0.79 ± 0.05 0.32 ± 0.79 0.74 ± 0.33 0.49	1.3 ± 0.8 8.5 ± 1.4 1.4 ± 0.1 0.10 ± 0.02 0.42 ± 0.02 0.16	7.0 ± 1.1 0.68 ± 0.04 0.80 ± 0.03 0.10 ± 0.27 0.54 ± 0.38 0.37	4.5 ± 2.3 0.98 ± 0.10 0.78 ± 0.08 0.5 ± 3.6 0.75 ± 0.75 0.24	not possible to fit the data (no convergence)
Model 1a Dual porosity medium; non–linear sorption ($N_f = N_p = 0.65$, fixed)	$a_L \cdot 10^3$ $K_f \cdot 10^4$ $K_p \cdot 10^3$ $\chi^2_{min} \cdot 10^5$	[m] $[\mathrm{mol}^{0.35}\mathrm{m}^{-0.05}]$ $[\mathrm{mol}^{0.35}\mathrm{m}^{1.95}\mathrm{kg}^{-1}]$ [–]	0.091 ± 0.047 0.38 ± 0.02 19.4 ± 0.2 0.14	0.82 ± 0.11 0.33 ± 0.02 4.3 ± 0.1 0.18	0.08 ± 0.14 0.010 ± 0.005 0.29 ± 0.01 0.28	3.3 ± 0.3 0.13 ± 0.01 0.11 ± 0.02 0.38	10 ± 1 0.26 ± 0.02 1.5 ± 0.3 1.29	4.3 ± 0.3 0.18 ± 0.01 0.092 ± 0.012 0.33	4.2 ± 0.4 0.34 ± 0.02 0.21 ± 0.02 0.24	not possible to fit the data (no convergence)
Model 2 Dual porosity medium; linear sorption	$a_L \cdot 10^3$ R_f $K_d \cdot 10^3$ $\chi^2_{min} \cdot 10^5$	[m] [–] $[\mathrm{m}^3\mathrm{kg}^{-1}]$ [–]	0.05 ± 0.23 6.4 ± 1.5 258 ± 9 1.2	0.32 ± 0.10 7.0 ± 0.8 70 ± 2 0.47	3.1 ± 3.7 8.3 ± 8.2 7.0 ± 4.4 1.5	2.7 ± 0.6 11 ± 2 2.3 ± 0.4 0.61	4.3 ± 4.5 22 ± 21 13 ± 10 1.28	6.2 ± 0.6 47 ± 3 4.4 ± 0.7 0.42	5.2 ± 0.8 149 ± 18 5.1 ± 0.3 0.23	30 ± 4 750 ± 70 0.086 ± 0.050 0.24
Model 3 Equivalent porous medium; non–linear sorption	$a_L \cdot 10^3$ $K_f \cdot 10^4$ N_f $\chi^2_{min} \cdot 10^5$	[m] $[\mathrm{mol}^{1-N_f}\mathrm{m}^{3N_f-2}]$ [–] [–]	18 ± 6 2.8 ± 0.2 0.50 ± 0.04 5.7		326 ± 129 1.1 ± 0.2 0.28 ± 0.07 6.2		146 ± 83 1.5 ± 0.2 0.45 ± 0.08 8.5		64 ± 31 0.70 ± 0.05 0.43 ± 0.06 0.53	
Model 4 Single porosity medium; linear sorption	M $a_L^{(j)} \cdot 10^3$ $R_f^{(j)}$ $\alpha^{(j)}$	[–] [m] [–] [–]	3 6 / 8 / 10 40 / 200 / 1000 0.49 / 0.35 / 0.16		3 5 / 8 / 10 15 / 90 / 1000 0.37 / 0.40 / 0.23		3 12 / 12 / 12 70 / 450 / 2000 0.43 / 0.23 / 0.34		2 10 / 10 250 / 1200 0.62 / 0.38	

Table 6: Fitted parameters, their standard deviations and the minimum values of the χ^2 merit function. The (upper) summation index has been omitted for models 1 to 3.

Model 1: (Dual porosity medium, non–linear sorption, 5 free parameters)

In general, this model gives reasonable fits (see Figures 2 – 5) for both geometries, but for a few cases some parameters are not compatible with independent experimental data [12] (N_f = 1.1; N_p = 0.46 for the sample BOE856R and fracture geometry) or are unphysical (e.g. for sample BOE856R2 and fracture geometry: N_f = 1.4; N_p = 0.42).
For the Böttstein core BOE1093, modelled as a vein network, it was not possible to get an acceptable fit. For every sample, we got a strong correlation between the Freundlich coefficient K_p and the exponent N_p. This is not the case for the surface sorption parameters K_f and N_f. Therefore we fixed both exponents to the experimental value of 0.65 [12] a procedure which we refer to as model 1a.

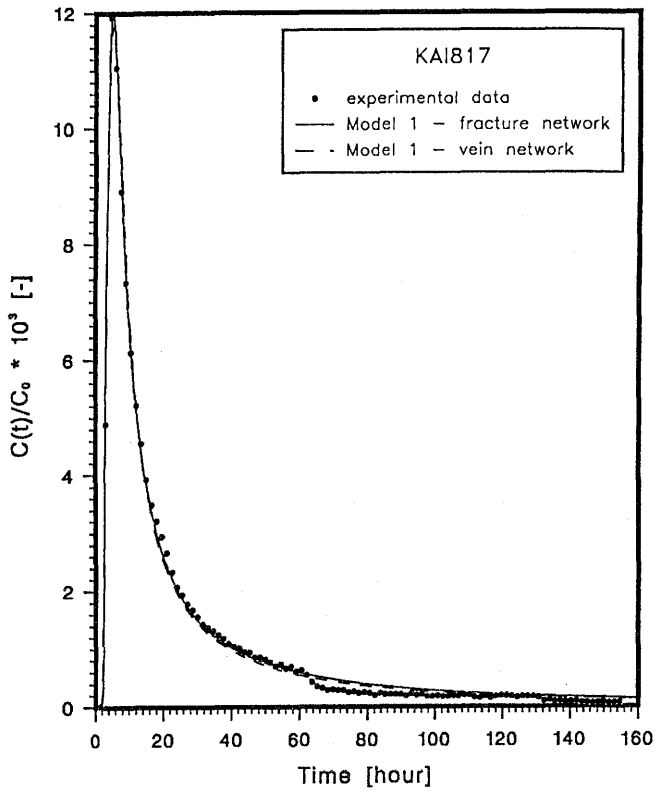

Figure 2: Best fits using model 1 for the core KAI817 with both alternative flow–path geometries.

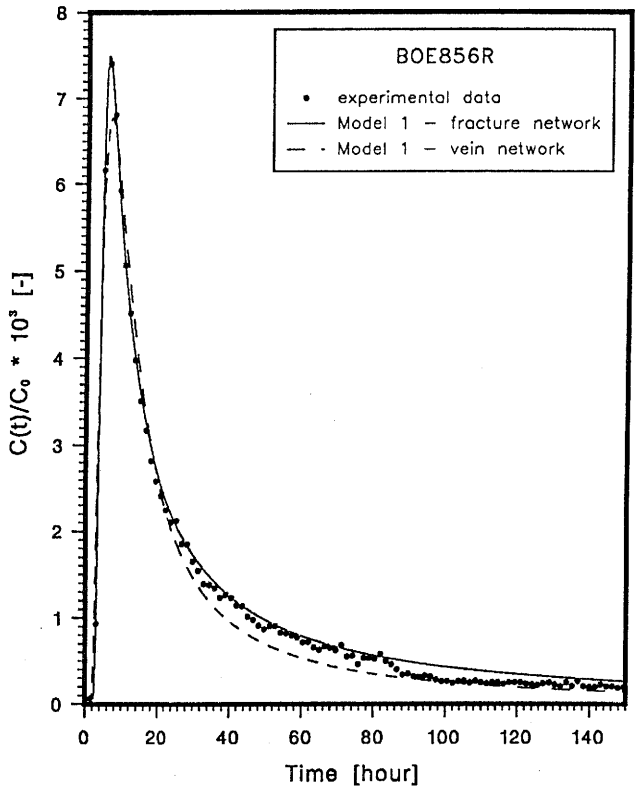

Figure 3: Best fits using model 1 for the core BOE856R with both alternative flow–path geometries.

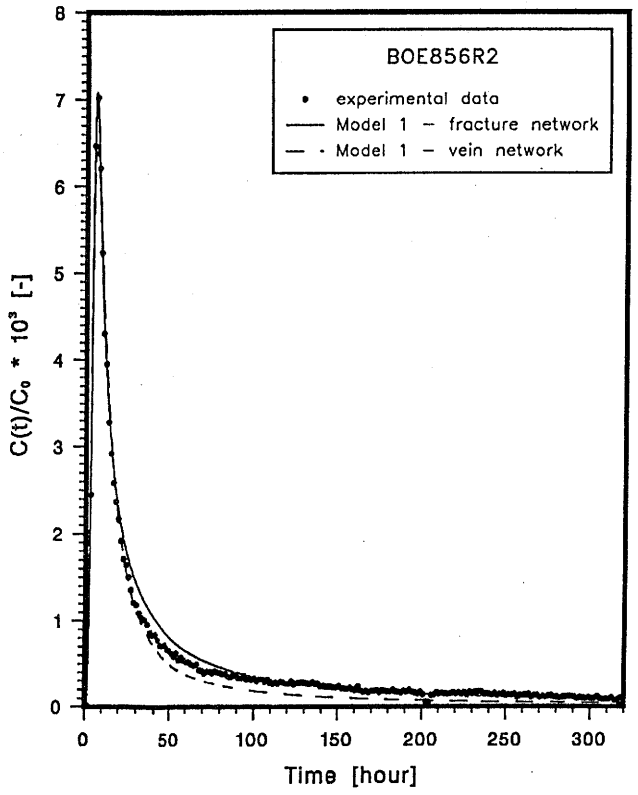

Figure 4: Best fits using model 1 for the core BOE856R2.

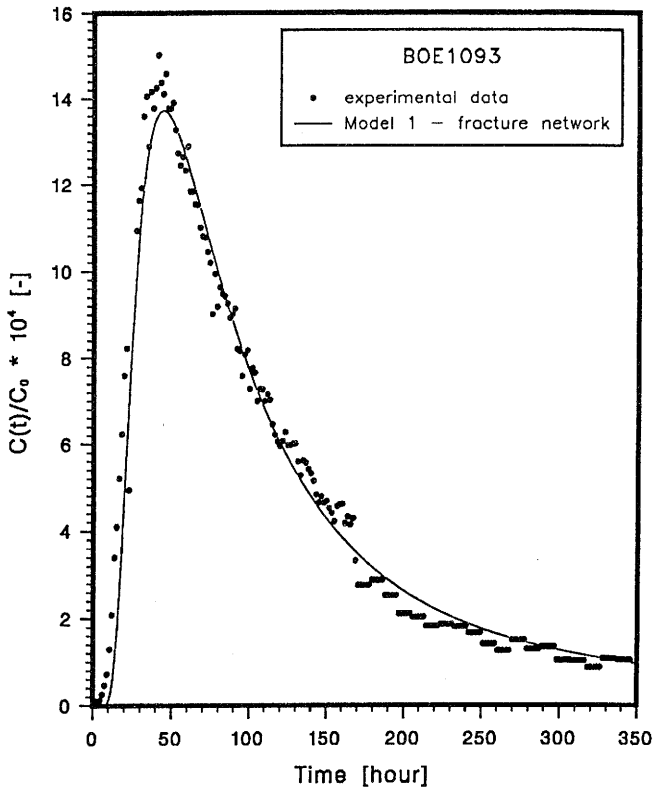

Figure 5: Best fit using model 1 for the core BOE1093.

Model 1a: (Dual porosity medium, non–linear sorption, 3 free parameters)

Despite having fixed both Freundlich exponents to a value of 0.65, the model reproduces the experimental data nearly as well as for model 1. This is illustrated in Figures 6 – 9 below. When decreasing the number of free parameters, the variability of the fit parameters becomes larger and the parameters have smaller standard deviations. Compared to model 1 the χ^2_{min}–values are smaller, but only in the vein flow cases. This may be a hint that convergence was not complete for some of model 1 runs. In fact χ^2_{min} for model 1a should be an upper limit for that of model 1. Again, as in model 1, for the bore core BOE1093 assuming a vein network, no reasonable fit was possible.

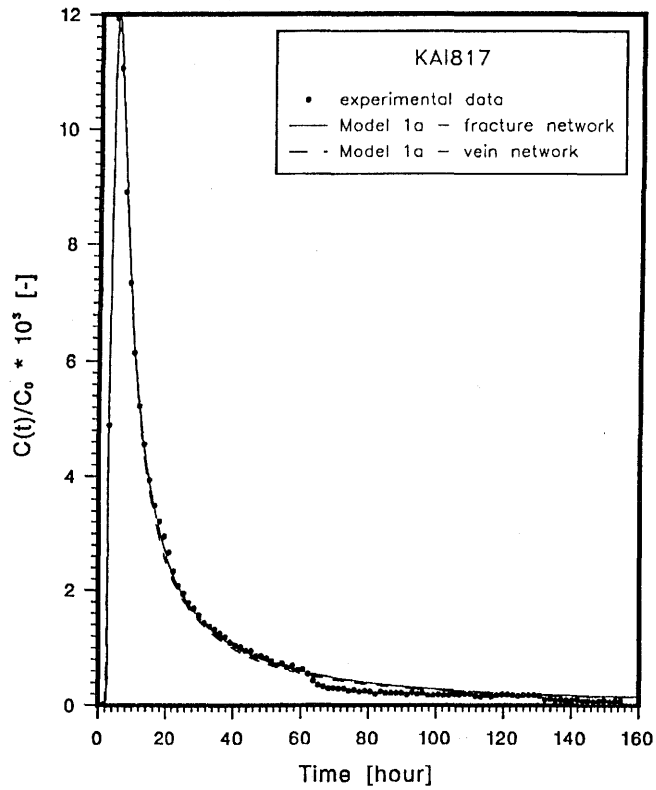

Figure 6: Best fits using model 1a for the core KAI817 with both alternative flow–path geometries.

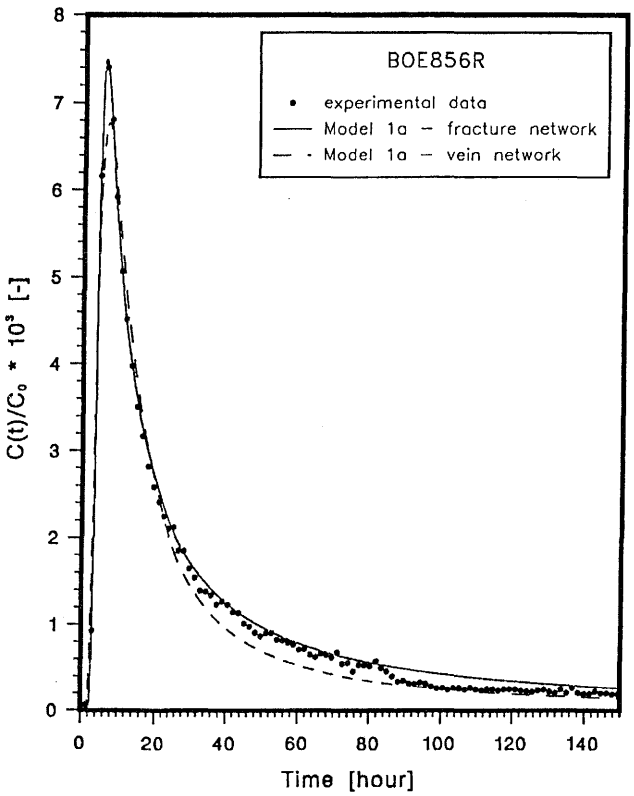

Figure 7: Best fits using model 1a and for core BOE856R with both alternative flow–path geometries.

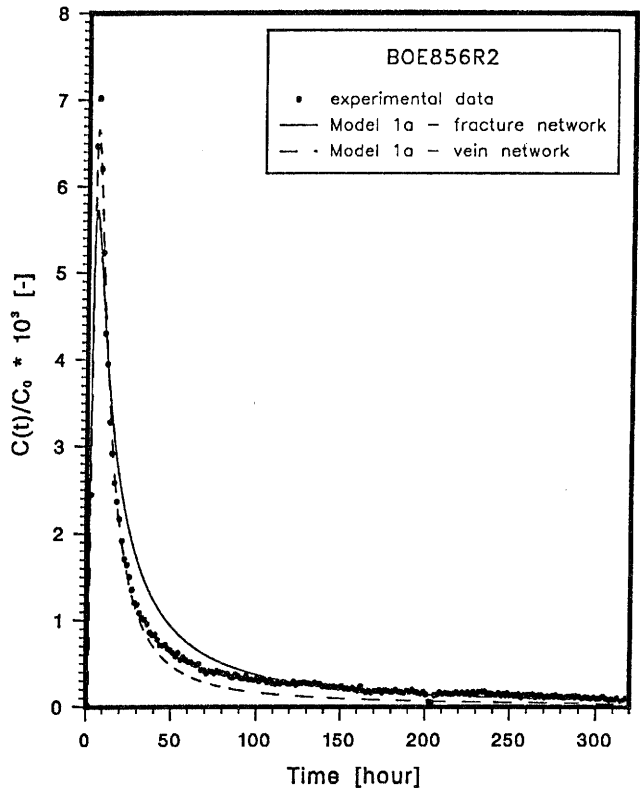

Figure 8: Best fits using model 1a for the core BOE856R2.

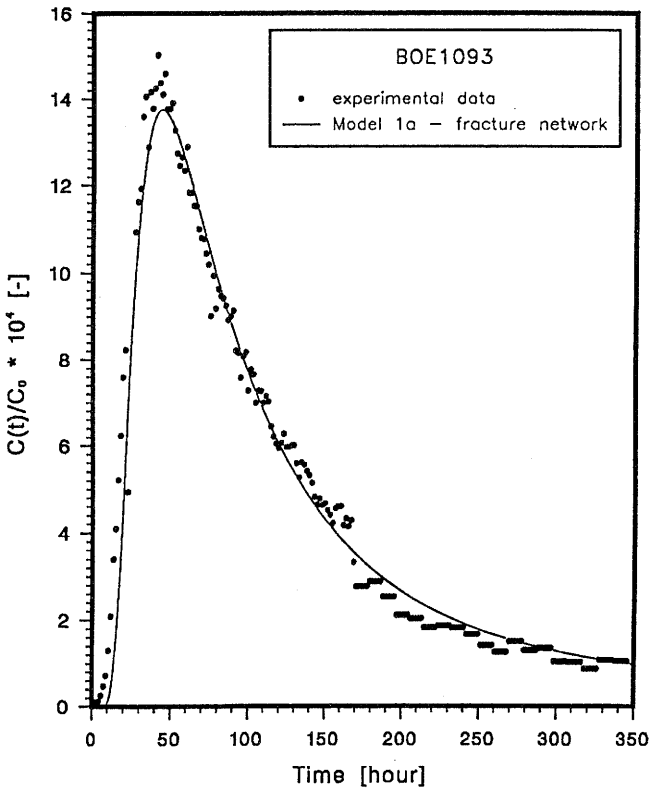

Figure 9: Best fit using model 1a for the core BOE1093.

Model 2: (Dual porosity medium, linear sorption, 3 free parameters)

In all four cases, the best fits for model 2 are only slightly less good than those for model 1. However, one notes that model 2 – in contrast to model 1 – is not able to reproduce the peak concentration value for the samples KAI817, BOE856R and BOE8562, respectively. Compared to former results [2], where fitting has been carried out by eye, one gets significantly smaller values for the longitudinal dispersivity and also for the retention factor R_f in the fracture/vein.
For BOE1093 and a vein network, large values arise for a_L and R_f, whereas the K_d–value is very small. According to [13] the longitudinal dispersivity a_L corresponds to the size of the heterogeneity of the medium at the microscopic scale. Hence a dispersivity, even greater than the length of the rock sample, is unreasonable; a REV cannot be defined and the macroscopic model breaks down.
All 2D–models (model 1, 1a and 2) show a tendency for an increased longitudinal dispersivity a_L towards a vein network. A greater dispersivity counteracts stronger retardation due to increased matrix diffusion in the case of vein networks.

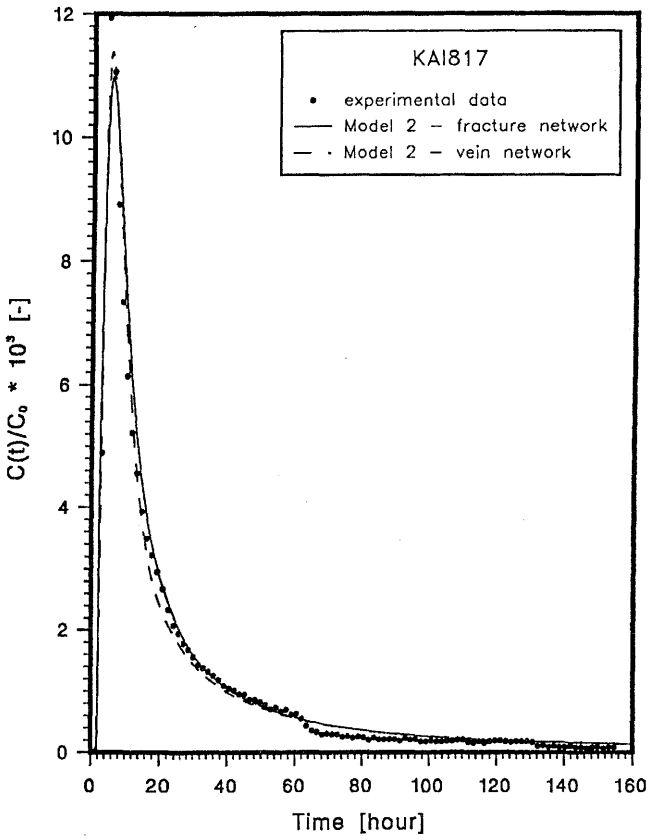

Figure 10: Best fits using model 2 for the core KAI817 with both alternative flow–path geometries.

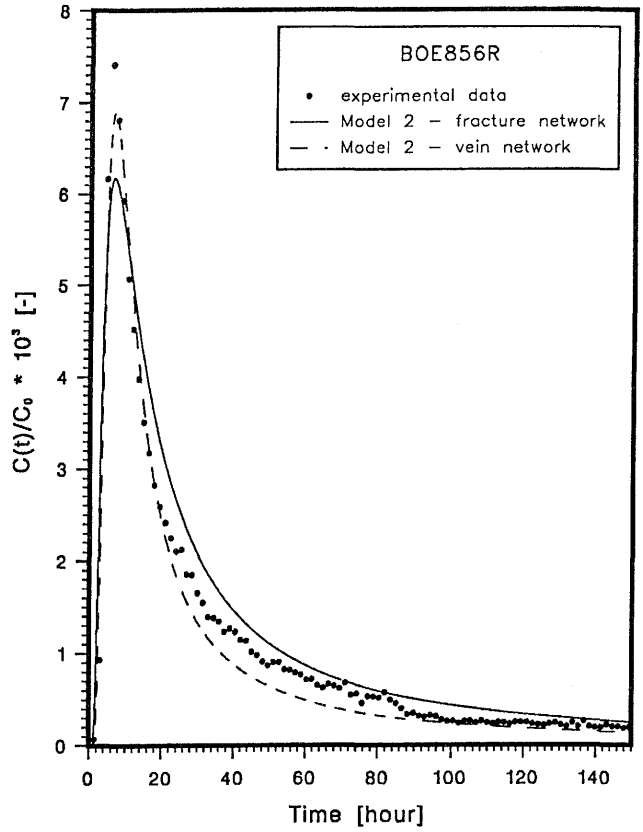

Figure 11: Best fits using model 2 for the core BOE856R with both alternative flow–path geometries.

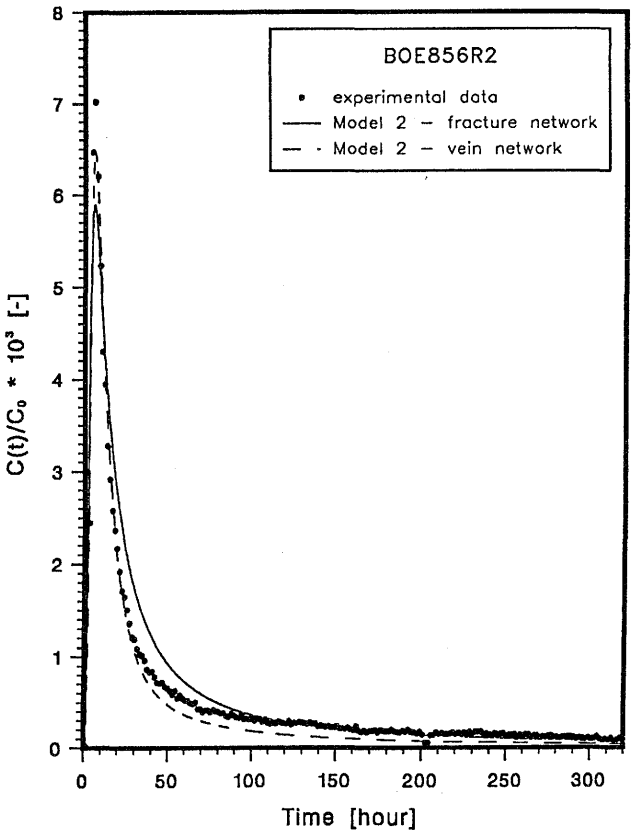

Figure 12: Best fits for model 2 for the core BOE856R2.

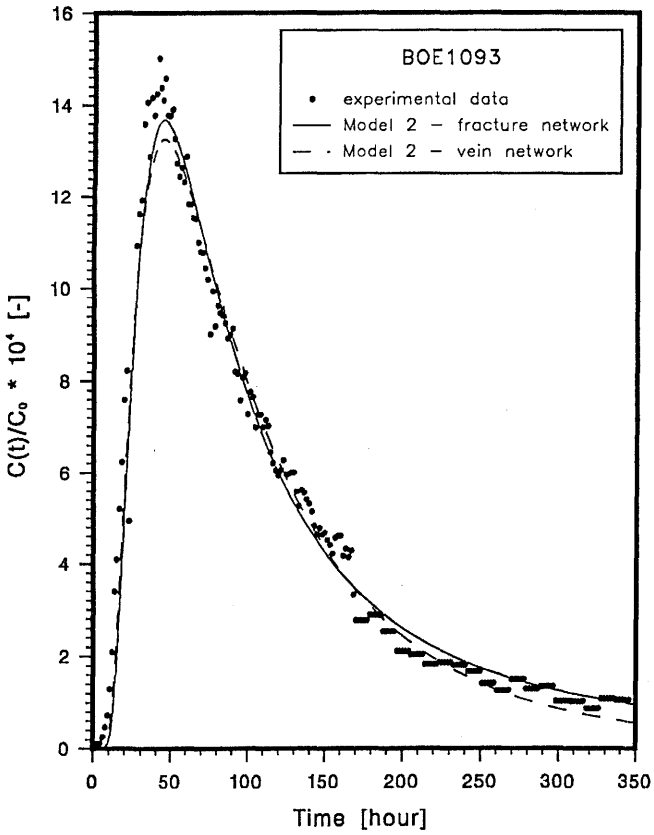

Figure 13: Best fits for model 2 for the bore core BOE1093.

Model 3: (Equivalent porous medium, non–linear sorption, 3 free parameters)

For all four core samples we get clearly worse fits than for all the models discussed before. This is demonstrated in Figures 14 – 17.
Examining the extracted parameter values, we note that generally the longitudinal dispersion length becomes extremely large, in contradiction to expectations and the application of the macroscopic model becomes doubtful. Also the values of the Freundlich exponent are rather small for all samples. From the fits, one sees that the tailing part of the break–through curves in particular cannot be reproduced by the model.

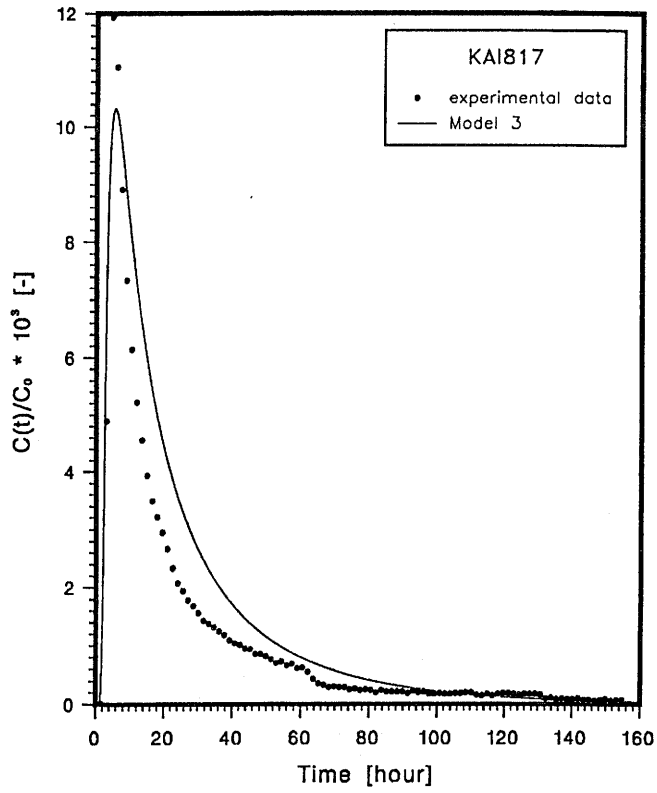

Figure 14: Best fit using model 3 for the core KAI817.

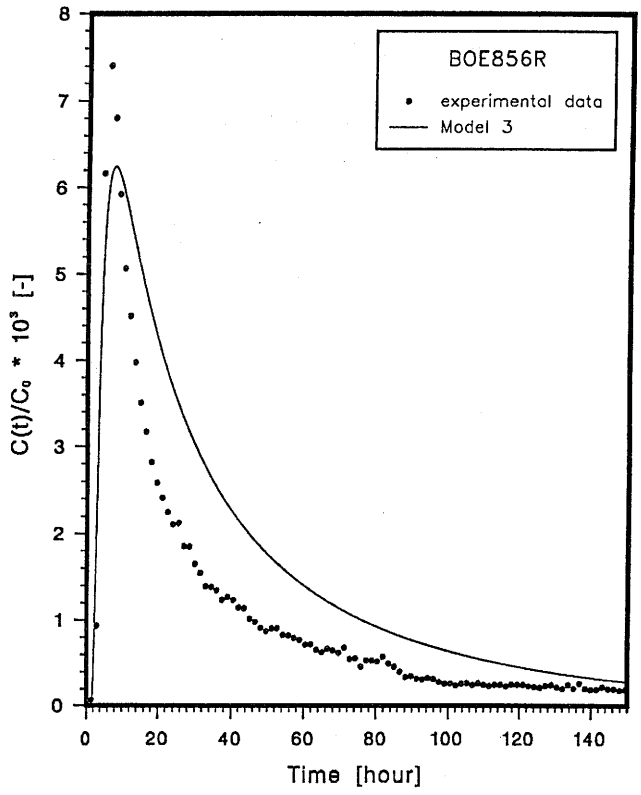

Figure 15: Best fit using model 3 and for the sample BOE856R.

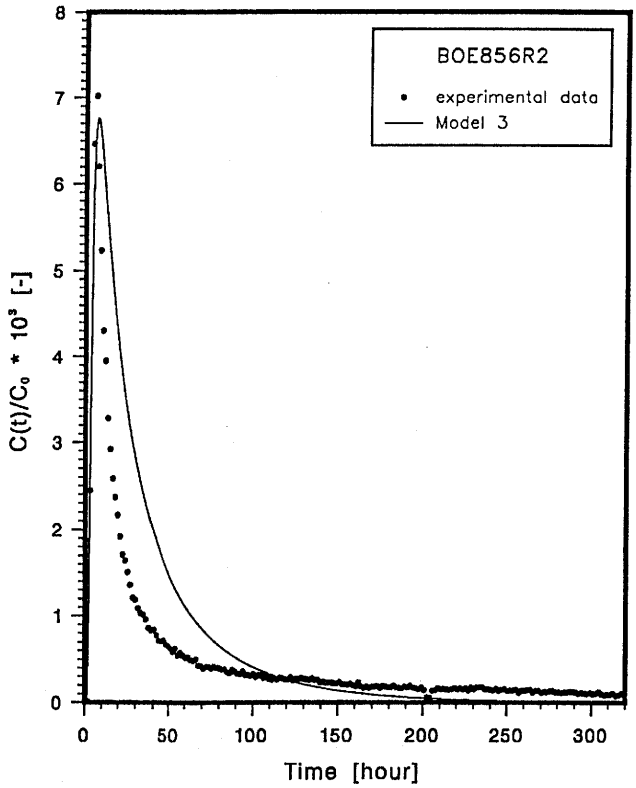

Figure 16: Best fit using model 3 for the core BOE856R2.

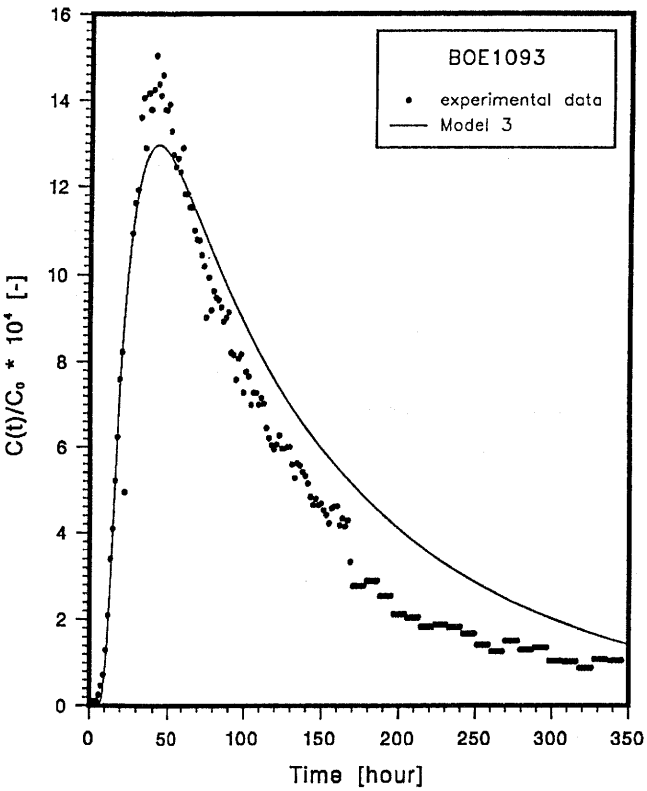

Figure 17: Best fit using model 3 for the core BOE1093.

Model 4: (Superimposed equivalent porous media, linear sorption, $3M$-1 free parameters)

This model fits every break–through curve very well (see Figures 18 – 21) and the extracted parameter values are not unreasonable. The number of fracture/vein families necessary to fit the experiments reasonably well is two or three.

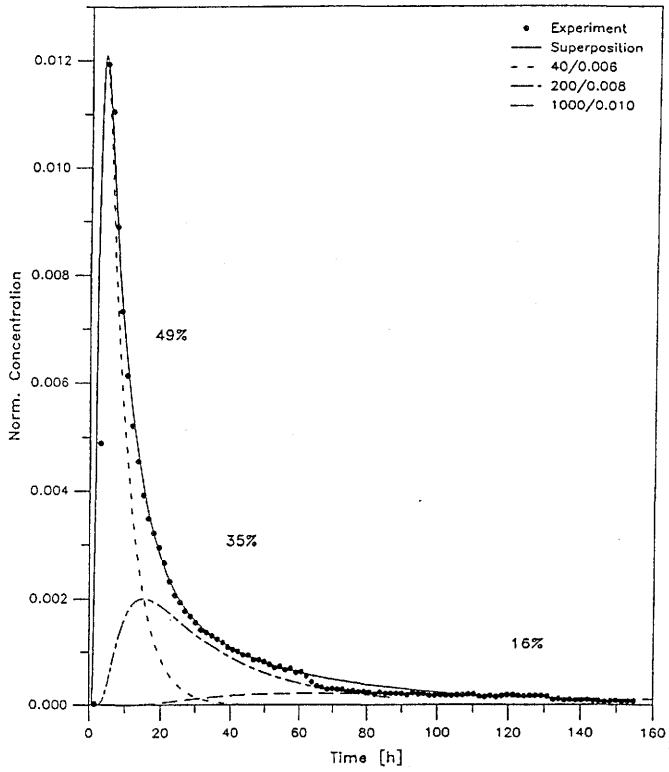

Figure 18: Best fit using model 4 for the core KAI817. The numbers at curves give the percent contribution of each fracture/vein family to the total concentration. Also given are the fitted valued R_f [–] and a_L [m] for the various families.

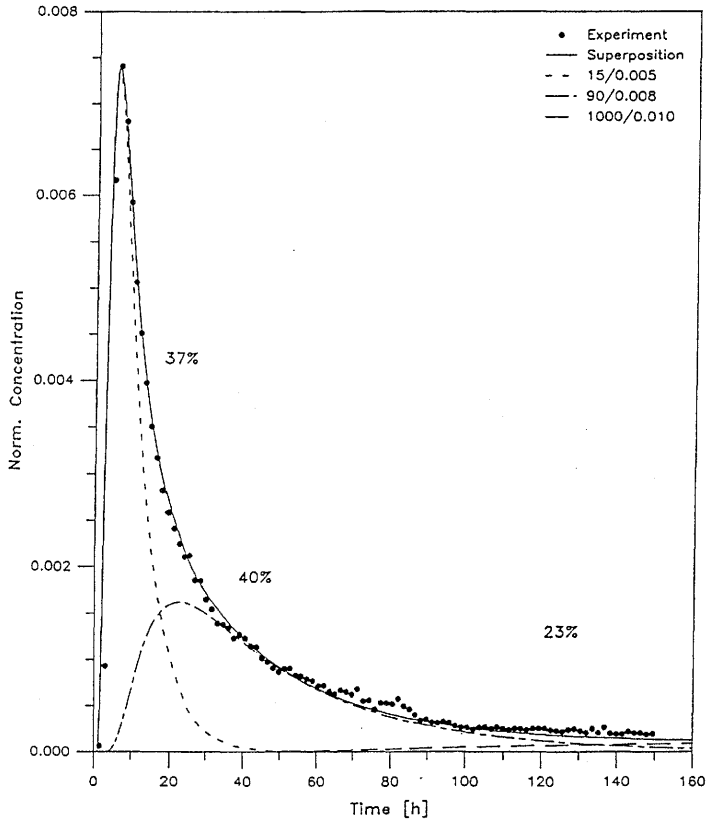

Figure 19: Best fit using model 4 for the core BOE856R. See also caption to Figure 18.

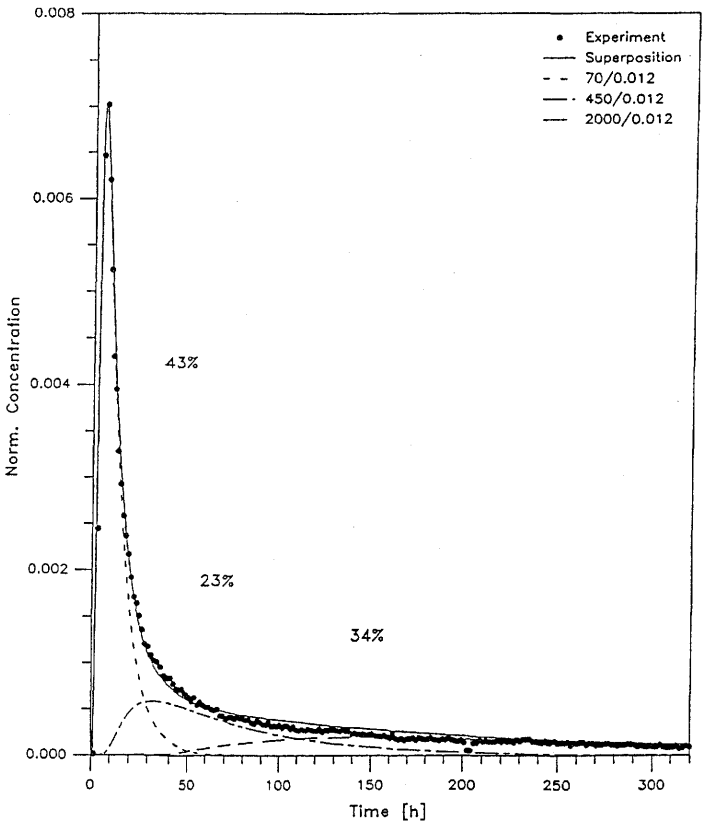

Figure 20: Best fit using model 4 for the core BOE856R2. See also caption to Figure 18.

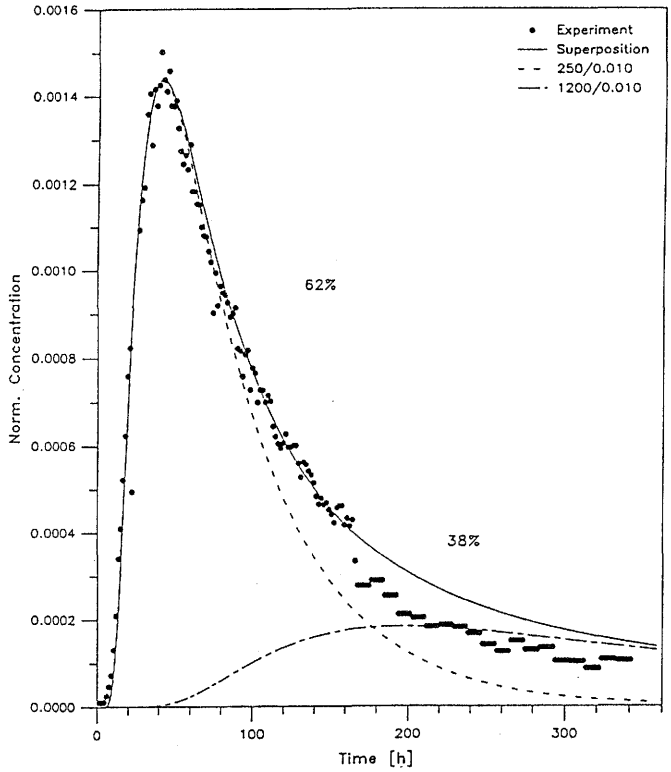

Figure 21: Best fit using model 4 for the core BOE1093. See also caption to Figure 18.

4.2 Mechanisms

Two questions can be asked when interpreting the case 1b experiments.

- First, is matrix diffusion, or rather diffusion into dead–end pores, an important process for these short–term experiments.
- Second, is the non–linearity of uranium sorption at the relevant concentration level, albeit not measured for precisely the same rock material, an important feature.

The first question can clearly be answered. A single porosity medium calculation does not give a satisfactory fit, even when taking into account the non–linearity of sorption, which enhances the tailing part of the break–through curve to some extent (model 3). From a safety assessment point of view this is gratifying since diffusion into extended pore spaces and sorption onto inner matrix surfaces represent efficient retardation mechanisms for transported radionuclides. In this context it is also worth mentioning that the very existence of water flow through the cores and the α–autoradiographs are proof of a strongly interconnected pore network in a rock material which would be considered as rock matrix in the framework of a safety analysis. However, it must be recognised that the samples did undergo decompression and compression cycles. Model 4 can, of course, fit the experimental results by assuming a sufficiently large member of flow channels. However, the individual parameters will never be assessable to a separate evaluation. This, together with its greater complexity, are the main arguments against model 4.

The answer to the second question is not so clear–cut. For the bore core KAI817, the fits are somewhat better with a non–linear isotherm. The values of K_p, the Freundlich coefficient in the rock matrix, are high, but the core originates from a gneiss and not from a granite. A decision as to whether sorption is linear or non–linear can hardly be made on the basis of these experiments, taking into account the inherent problems. The same is also true when looking at the upper Böttstein cores, BOE856R and BOE856R2 individually. Here, however, we may invoke a further argument. The two bore cores originate from almost the same depth differing by only 13 cm, and show no apparent differences in their characterisation. We might, therefore, hypothesise that the parameters extracted from the break–through curves should also be similar for these two cores. Disregarding fits which are unsatisfactory because the fit quality is bad and parameters have extremely large errors (model 2, fracture geometry) or parameters are unphysical (model 1, fracture geometry), the model with non–linear sorption (Model 1/1a) is to be preferred over the model with linear sorption (Model 2).

4.3 Effect of different upstream boundary conditions

In this section, we discuss briefly some effects which are related to the specific experimental design and which make interpretation of the experimental data quite difficult.

- As mentioned earlier (see also page 9 and [14]) the tracer pulse spends some time (the transit–time) Δt in the "dead–volume". The dead–volume consists of the internal volume of those parts of the infiltration apparatus between the injection point (upstream) and the measurement point, but without the sample. The transit–time is not a well defined value because the tracer enters the rock–sample continuously during its passage along the spiral groove of the end–piece, giving rise to a curved (smeared) tracer front in the sample. The duration of tracer injection T_L is not well defined since the input function is not a simple rectangular pulse.
- Due to dispersive effects within the dead–volume, the experimental input function may be even more complex.
- As a further point we mention the problem of mass conservation at the upper boundary. Assuming a time dependent input function $C_0(t) = C_0 \cdot f(t)$ for the nuclide release over the period T_L [s], we obtain the following expression for the total mass m entering the sample through the boundary:

$$\begin{aligned} m &= q \cdot F \cdot \int_0^{T_L} C_0(t)dt = \\ &= \epsilon_f \cdot F \left[\int_0^{T_L} v_f \cdot C_f(z=0,t)dt - \int_0^{T_L} v_f \cdot a_L \frac{\partial C_f(z,t)}{\partial z} \Big/_{z=0} \; dt \right] \end{aligned} \tag{4.1}$$

  where F [m^2] is the cross–sectional area of the sample. In neglecting the dispersive term of the right hand side of eq. (4.1), as is done using eq. (3.8), one violates the mass conservation over the boundary. (The value of the longitudinal dispersivity may be very small but the derivative may deviate considerably from zero during the period of injection).

To study the influence of the more appropriate upstream boundary condition (4.1) we have repeated the fitting procedure for one bore core (BOE856R) using all the models – except, of course for model 4 – and both alternative flow path geometries (for model 1, 1a and 2). For the sake of simplicity and due to lack of data, we assumed as for the previous calculations, a rectangular pulse input function. The results are presented in Table 7 below.

Model	Parameter		Up–stream boundary condition			
			$C_f(z=0) = C_0 \cdot \Theta(T_L - t)$		$\left(C_f - a_L \frac{\partial C_f}{\partial z}\right)_{z=0} = C_0 \cdot \Theta(T_L - t)$	
			fracture flow	vein flow	fracture flow	vein flow
Model 1 Dual porosity medium; non–linear sorption	$a_L \cdot 10^3$ $K_f \cdot 10^4$ N_f $K_p \cdot 10^3$ N_p $\chi^2_{min} \cdot 10^5$	[m] $[\text{mol}^{1-N_f}\text{m}^{3N_f-2}]$ [–] $[\text{mol}^{1-N_p}\text{m}^{3N_p}\text{kg}^{-1}]$ [–] [–]	0.36 ± 0.24 0.36 ± 0.06 1.1 ± 0.1 0.079 ± 0.012 0.46 ± 0.03 0.091	4.3 ± 1.2 0.37 ± 0.04 0.79 ± 0.05 0.32 ± 0.79 0.74 ± 0.33 0.49	0.51 ± 0.20 0.23 ± 0.03 0.98 ± 0.03 0.047 ± 0.009 0.39 ± 0.03 0.079	3.3 ± 1.0 0.086 ± 0.004 0.63 ± 0.03 0.026 ± 0.078 0.58 ± 0.36 0.49
Model 1a Dual porosity medium; non–linear sorption ($N_f = N_p = 0.65$, fixed)	$a_L \cdot 10^3$ $K_f \cdot 10^4$ $K_p \cdot 10^3$ $\chi^2_{min} \cdot 10^5$	[m] $[\text{mol}^{0.35}\text{m}^{-0.05}]$ $[\text{mol}^{0.35}\text{m}^{1.95}\text{kg}^{-1}]$ [–]	0.08 ± 0.14 0.010 ± 0.005 0.29 ± 0.01 0.28	3.3 ± 0.3 0.13 ± 0.01 0.11 ± 0.02 0.38	19 ± 6 0.20 ± 0.03 0.095 ± 0.030 2.9	3.0 ± 0.4 0.095 ± 0.005 0.047 ± 0.003 0.50
Model 2 Dual porosity medium; linear sorption	$a_L \cdot 10^3$ R_f $K_d \cdot 10^3$ $\chi^2_{min} \cdot 10^5$	[m] [–] $[\text{m}^3\text{kg}^{-1}]$ [–]	3.1 ± 3.7 8.3 ± 8.2 7.0 ± 4.4 1.5	2.7 ± 0.6 11 ± 2 2.3 ± 0.4 0.61	0.01 ± 0.22 0.50 ± 0.61 4.0 ± 0.2 1.4	1.7 ± 0.4 7.4 ± 0.8 1.2 ± 0.1 0.75
Model 3 Equivalent porous medium; non–linear sorption	$a_L \cdot 10^3$ $K_f \cdot 10^4$ N_f $\chi^2_{min} \cdot 10^5$	[m] $[\text{mol}^{1-N_f}\text{m}^{3N_f-2}]$ [–] [–]	326 ± 129 1.1 ± 0.2 0.28 ± 0.07 6.2		299 ± 447 0.041 ± 0.021 0.30 ± 0.16 11	

Table 7: The influence of a changed up–stream boundary condition on the fitted parameters for the rock sample BOE856R using models 1 to 3.

Model 1: (Dual porosity medium, non–linear sorption, 5 free parameters)

For fracture flow, the parameter values are comparable to those from the previous calculation. Again the Freundlich exponent in the fracture is unrealistic high (approximately unity) with respect to [12], whereas in the matrix the exponent becomes even smaller (N_p = 0.39 instead 0.46). Nevertheless the calculated break–through curve fits the experimental data very well.
In the case of vein flow, the Freundlich coefficients become essentially smaller, but they may still be acceptable, consistent with data from independend batch–sorption experiments [12].

Model 1a: (Dual porosity medium, non–linear sorption, 3 free parameters)

For fracture flow the value of the longitudinal dispersivity becomes now unrealistically high ($a_L \sim 1.9$ cm!) (see also [13]) and the value of the χ^2_{min} merit function is an order of magnitude greater than in the previous calculation.
For vein flow, the values of the best fit parameters are up to a factor of about 2 smaller but they seem reasonable.
This, together with the remarks concerning model 1, may indicate that, for the bore core BOE856R, the vein geometry may be more appropriate than the fracture geometry.

Model 2: (Dual porosity medium, linear sorption, 3 free parameters)

The above conclusion is reinforced by the best fit parameter values for model 2. For fracture flow the values for a_L and R_f are still undetermined, whereas for vein flow the values seem reasonable and have much smaller error bars. In general, for both flow–path geometries, the values become smaller in the case of a mixed upstream boundary condition.

Model 3: (Equivalent porous medium, non–linear sorption, 3 free parameters)

As in the previous calculation, with a mixed upstream boundary condition the parameter value for a_L is still undetermined, the Freundlich exponent is again very low and the fit is even worse. We conclude that the modified boundary condition cannot support the model. It seems that model 3 is not able to reproduce experimental data in a satisfactory way.

Disregarding the fracture flow geometry, again on grounds of inconsistent parameters ($N_f \approx 1$ for model 1, a_L = 1.9 cm for model 1a), the flow boundary condition does not yield strongly different parameters compared to the concentration boundary.

4.4 Penetration depth for matrix diffusion

The numerical problem of discretisation in the direction of matrix diffusion is strongly related to the question of the penetration depth for matrix diffusion. It is obvious that, if the concentration profile in the rock matrix is badly represented due to an inappropriate discretisation, this will strongly influence the calculated break–through curves at the downstream boundary, because matrix diffusion acts as an important retardation mechanism for released nuclides.
For all calculations we have chosen the distance to the no–diffusive–flux boundary $D^{(j)}$ to be sufficiently large, that its value does not influence the numerical solution of the transport equations. $D^{(j)}$ represents a maximum possible penetration depth into the matrix, but without an idea of the actual penetration depth, the extent of the discretisation mesh and its mesh size may be completely inadequate, resulting in crude time histories for the nuclide concentration.
In the case of fracture flow (planar (x, z)–geometry), there is an analytical expression for the actual penetration depth [15]. The $1/e$–concentration level $C(D^{(j)}_{1/e})/C(x = 0) = 1/e$ is reached at:

$$D^{(j)}_{1/e} \approx 2\sqrt{\frac{\epsilon_p^{(j)} D_p^{(j)}}{\overline{\rho} \cdot K_d^{(j)}} \cdot \Delta t} \tag{4.2}$$

and the 1% concentration treshold $C(D_{0.01}^{(j)})/C(x = 0) = 0.01$ at:

$$D_{0.01}^{(j)} \approx 4\sqrt{\frac{\epsilon_p^{(j)} D_p^{(j)}}{\overline{\rho} \cdot K_d^{(j)}} \cdot \Delta t} \tag{4.3}$$

where Δt [s] is the contact time between the migrating nuclide pulse and the rock matrix.

Similar simple analytical expressions for vein flow (cylindrical (r, z)–geometry) are not known.
In figure 22, we have plotted the calculated concentration profile and also the values for the diffusive flux into the rock matrix using model 2 (dual porosity medium, linear sorption) for the bore core BOE856R with both flow path geometries. The smoothness of the curves indicates the density of the discretisation points. A positive sign of the diffusive flux signifies diffusion into the rock matrix, whereas a negative sign means a movement of mass/activity back towards the fracture/vein. After 8 hours, close to the inlet ($z = 0.52$ cm) the diffusive flux has become partially negative, indicating that the moving nuclide pulse in the fracture/vein has already passed and diffusion back across the interface occurs. On the other hand, at 1.00 and 1.41 cm, the values of the flux are always positive and therefore only diffusion of the tracer into the rock matrix occurs at these positions.
At 98.6 hours after the injection, the concentration profile in the matrix has decreased at least an order of magnitude due to the spreading of the nuclide distribution through the rock matrix and subsequent backdiffusion to the flow path. The penetration depth has now reached a few tenths of a millimeter.
The interpretation of such plots from different locations and at different times may be helpfull in finding a suitable discretisation scheme, especially for vein flow systems.

4.5 Geometry of water conducting zones

Generally, the best fits for the individual break–through curves do not discriminate clearly between fracture and vein geometry for the water conducting zones. This is especially surprising in the case of KAI817 where a branching fracture is seen in the photographs and in the α–autoradiographies. A closer inspection of the autoradiographs shows, however, that a large part of the activity is irregularly distributed over the core cross sections. A combination of both flow geometries could therefore be a more realistic picture. For the deep Böttstein core, BOE1093, in the case of vein geometry a fit was either not possible (models 1 and 1a) or yielded parameters inconsistent with independent information. This might be an indication that fracture geometry is more appropriate.
For the upper Böttstein cores, BOE856R and BOE856R2, the situation is more complex. Let us consider core BOE856R. For model 2, the parameters for a fracture geometry are largely undetermined, in contrast to a vein geometry which also yields a better fit; the mean values are reasonable in both cases. For model 1, the fracture geometry yields a better fit; however, the extracted parameters, especially the Freundlich exponents, are judged to be inconsistent. For model 1a, a_L can not be extracted in the fracture geometry case, but the remaining parameters are reasonable for both geometries. For bore core BOE856R2, again, parameters for a fracture geometry are undetermined and the fit is better for a vein geometry when considering model 2. For model 1 both geometries produce a comparable fit quality, but the parameters of the fracture calculation are inconsistent with independent information. For model 1a vein geometry yields a better fit, but the parameters are sensible for both geometries. Taking all together, a vein geometry is judged to be a preferable flow path representation. The α–autoradiographs do not help in discriminating the geometries.
The flow path geometry is an important parameter [7] in a repository safety assessment. However, in such a case the necessary information will come from geology site investigations. Hence, the difficulty in extracting geometries from the present case 1b experiments has no impact on use of transport models in safety analysis. In this context it is also noteworthy that in the framework of a safety assessment, the rock material used in these experiments would be considered as rock matrix rather than a dual porosity medium.

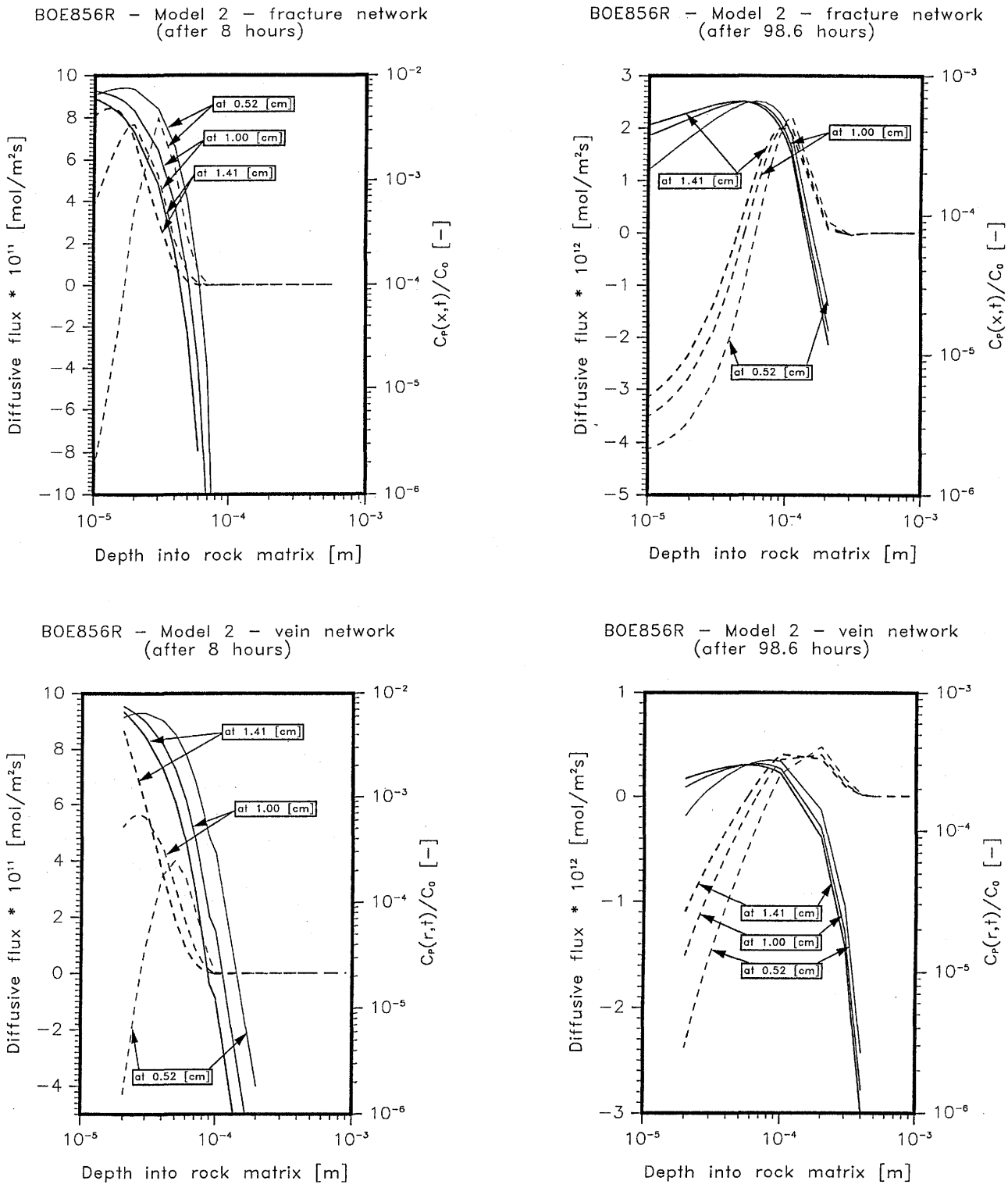

Figure 22: The relative nuclide concentration $C_p(s,t)/C_0$ (solid lines) and the diffusive flux $j_D = -D_p \partial C_p(s,t)/\partial s$ (dashed lines) in the rock matrix after t = 8 and 98.6 hours after the tracer injection; $s = \{x \text{ or } r\}$. The profiles are taken at z = 0.52, 1.00 and 1.41 cm, respectively, along the migration path as indicated in the plots. The calculations have been carried out for a dual porosity medium including linear sorption (model 2). The fracture half–width b is equal to 10^{-5} m and the vein radius $R = 2 \cdot 10^{-5}$ m. A direct comparison of the concentration profiles and the fluxes presented for the two geometries is not feasible because the K_d's are those of the best fits, which are different to each other and hence are also the effects of matrix diffusion.

4.6 Methodology: Fitting procedure

Compared to the previous modelling [2], where curves were fitted by eye, the automatic Marquardt–Levenberg procedure has two advantages. First, it yields an objective measure for the goodness of the fit and second, error estimates of the extracted parameters can be given. There are marked differences between the previous but fits–by–eye and the present automatic fits (Figure 23). The parameters do not agree within the error ranges, though both sets are reasonable with, perhaps, the exception of the dispersivity for BOE856R in the previous modelling. The reason of the differences is that, in the automatic fit, all data points are equally weighted and, in the fit by eye, the few data points in the peak region receive intuitively more weight.

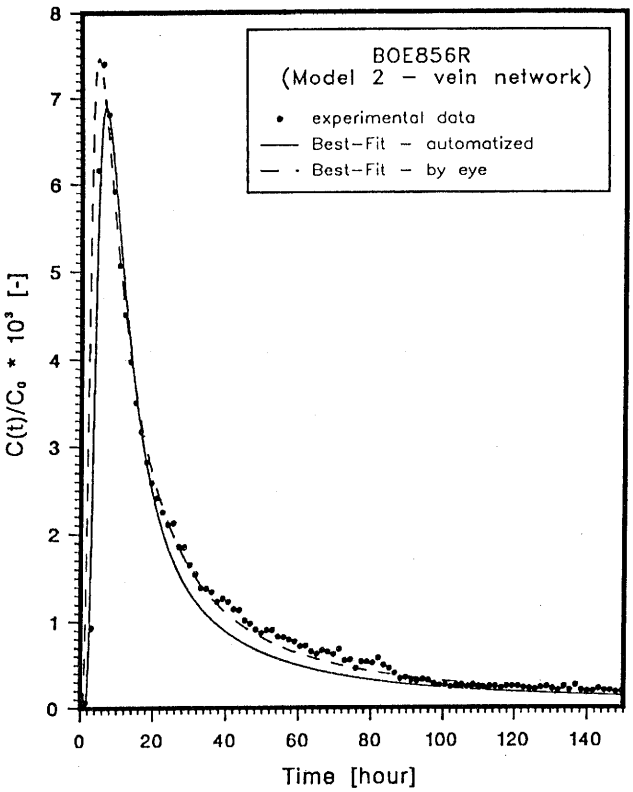

Figure 23:
Comparison of the Best fits (solid line – $\chi^2_{min} = 0.60 \cdot 10^{-5}$) and the fit–by–eye taken from [2] (dashed line – $\chi^2 = 3.1 \cdot 10^{-5}$) for the sample BOE856R using model 2 with a vein network.

5 Conclusions

We would first like to summarise the discussion presented in section 4.
The experimental information available for the break–through curves is not sufficient to determine all the parameters which enter the models. As an expedient, some of the parameters have been fixed by independent information and using common wisdom but, even then, parameters assumed to be independent might be correlated. Despite this unpleasant situation some conclusions are possible, especially when judging the values of the extracted parameters:

- Transport of radionuclides over distances in the order of centimetres is possible in samples of rock material which would be considered as rock matrix in a safety assessment. However, this conclusion is valid only, if fracturing during sampling can be neglected.
- A dual porosity model is more appropriate for the description of the experiments. It is matrix diffusion rather than the non–linearity of the isotherm which is needed to describe the tailing part of break–through curves.
- The geometry of water flow paths can rarely be determined. From a safety assessment point of view, this information may be irrelevant since the samples consist of matrix material.
- The sorption, as measured in static batch experiments, is not in contradiction to the information extracted from the dynamic infiltration when using an appropriate transport model.
- The parameters extracted by a fit–by–eye might deviate appreciably from those evaluated by an automatic fit procedure.

The possibility for more firm conclusions is strongly restricted by experimental difficulties and shortcomings, which need not be repeated here. However, some of the suggestions for further experimentation following from this modelling exercise need mentioning.

- First, material with clearly defined flow path geometry, e.g. with an open fracture, should be used.
- Second, break–through curves for several tracers should be obtained. One of them should be non–sorbing so that nuclide independent parameters can be extracted.
- The density of experimental points in the peak region should be sufficiently high such that an automatic fitting procedure gives that region sufficient weight (Or else the modeller could introduce a – subjective – weight function).
- Since the models, except model 4, predict parameter dependencies, the experimental conditions should be varied, e.g. the water velocities and the duration of the tracer input. Variation of sample length would give information concerning the notion of a REV and on the consistency of the dispersivity.
- Several different bore cores originating from the same location should be used.
- An appropriate groundwater should be used.
- Finally an appropriate laboratory support programme to measure sorption on relevant samples is essential.

We would like to note that many of these wishes from the modellers' side, including a redesign of the pressure cell endpieces, are being taken into account in PSI laboratory work subsequent to the experiments constituting case 1b.

Acknowledgements

We would like to acknowledge many helpful discussions within the INTRAVAL community. Thanks go especially to J. Carrera, W. Heer, I. McKinley, P. Zuidema and P. Smith for helpful discussions, to A. Zingg for performing the model 4 calculations and E. Curti and T. Karapiperis for the translations of the abstract. We would like to thank Miss R. Bercher for her tireless efforts in carefully typing the manuscript. This work is partially supported by NAGRA.

References

[1] "The International INTRAVAL Project, Background and Results", OECD/NEA, Paris 1990

[2] **Hadermann, J., Jakob, A.:** "Modelling small scale infiltration experiments into bore cores of crystalline rock and break–through curves", EIR-Bericht Nr. 622, Würenlingen, April 1987 and NTB 87–07, NAGRA, Baden, April 1987

[3] **Bischoff, K., Wolf, K., Heimgartner, B.:** "Hydraulische Leitfähigkeit, Porosität und Uranrückhaltung von Kristallin und Mergel: Bohrkern–Infiltrationsversuche", EIR-Bericht Nr. 628, Würenlingen, April 1987 and NTB 85–42, NAGRA, Baden, April 1987

[4] **Schmassmann, H., Balderer, W., Kanz, W., Pekdeger, A.:** "Beschaffenheit der Tiefengewässer in der zentralen Nordschweiz und angrenzenden Gebieten", NTB 84–21, NAGRA, Baden, August 1984

[5] **Bear, J.:** "Hydraulics of Groundwater", McGraw–Hill Book Company, 1979

[6] **Wernli, B., Bajo, C., Bischoff, K.:** "Bestimmung des Sorptionskoeffizienten von Uran(VI) an Grimsel– und Böttsteingranit", EIR–Bericht Nr. 543, Würenlingen, Februar 1985 und NTB 84–46, NAGRA, Baden, September 1984

[7] **Jakob, A., Hadermann, J., Rösel, F.:** "Radionuclide chain transport with matrix diffusion and non–linear sorption", PSI–Bericht Nr. 54, Würenlingen, November 1989 and NTB 90–13, NAGRA, Baden, February 1990

[8] **Hadermann, J., Rösel, F.:** "Radionuclide Chain Transport in Inhomogeneous Crystalline Rocks; Limited Matrix Diffusion and Effective Surface Sorption", EIR–Bericht Nr. 551, Würenlingen, Februar 1985 and NTB 85–40, NAGRA, Baden, February 1985

[9] IMSL–Library, Edition 10 (1987)

[10] **Skagius, K., Neretnieks, I.:** "Diffusivities in crystalline rock materials", in: Scientific Basis for Nuclear Waste Management IX, Vol. 50 (1985), Material Research Society, Pittsburgh, Pennsylvania, p. 73 – 80

[11] **Tang, D.H., Frind, E.O., Sudicky, E.A.:** "Contaminant Transport in Fractured Porous Media: Analytical Solution for a Single Fracture", Water Res. Res., Vol. 17, No. 3, p. 555 – 564, June 1981

[12] **Aksoyoglu, S., Bajo, C., Mantovani, M.:** "Sorption of U(VI) on granite", J. Radioanal. Nucl. Chem., Vol. 134 (1989), No. 2

[13] **Bear, J., Verruijt, A.:** "Modelling Groundwater Flow and Pollution", D. Reidel, Publishing Company, Dordrecht, Holland, 1987

[14] **Smith, P., Hadermann, J., Bischoff, K.:** "Dual–Porosity Modelling of Infiltration Experiments on fractured Granite", PSI–TM–41–90–02, Würenlingen und Villigen, January 1990

[15] **Neretnieks, I.:** "Diffusion in the Rock Matrix: An important factor in Radionuclide Retardation?", J. of Geophys. Res., Vol. 85, No. B8, p. 4379–4397, August 10, 1980